Williams College

Koh, Da-Yeon

2024 Physics Thesis

Construction of a Stabilized Laser for Cooling Strontium Ions

Advisor	Charlie Doret
Additional Advisor	
Access	None of the above
Contains Copyrighted Material?	No
Release Restrictions	release now
Authenticated Access	

Construction of a Stabilized Laser for Cooling Strontium Ions

by
Da-Yeon Koh

Professor Charlie Doret, Advisor

A thesis submitted in partial fulfillment
of the requirements for the
Degree of Bachelor of Arts with Honors
in Physics

WILLIAMS COLLEGE
Williamstown, Massachusetts
May 20, 2024

Abstract

The Doret lab has begun its efforts to trap and cool Strontium ions for the purpose of analog quantum simulation of heat transfer. A part of that effort has been making the 422nm laser, which addresses the $4S_{1/2} \leftrightarrow 5S_{1/2}$ cooling and fluorescence transition of Sr^{+}. The laser path is made suitable for electromagnetically-induced tranparency(EIT) cooling by having the ability to create two beams of appropriate polarization and frequency difference. The laser is frequency stabilized in reference to a transition in Rubidium. Lock-in detection on a Doppler-free absorption line from saturated absorption spectroscopy is used to create an error signal for PID locking. A homemade RF amplifier capable of modulating the frequency sent to an acousto-optical modulator was constructed as a part of this work. The stabilized laser will also enable other lasers to lock in reference to it via a Fabry-Perot cavity.

Executive Summary

In order to simulate the phenomenon of thermal rectification in mesoscopic systems, the Doret lab now plans to trap a new species of ions: strontium. This requires the construction of new lasers, vacuum systems, and a 3D Paul trap. One of the lasers probes the $5S_{1/2} \leftrightarrow 5P_{1/2}$ 422 nm transition of Sr^+, which is the fluorescence and cooling transition of the ion.

The aforementioned transition has a natural linewidth of $2\pi \times 20$ MHz. In order for the laser to be useful in cooling, it must be stabilized to an order of magnitude or more narrower ranger than this.The lab will also implement electromagnetically-induced tranparency (EIT) cooling for both Ca^+ and Sr^+ ions in the future. This thesis describes the construction of a frequency-stabilized laser capable of EIT cooling Sr^+ ions.

For the purpose of EIT cooling, we need to be able to generate two beams, coherent with each other, with slightly different frequencies, of π and σ^- polarizations. This is achieved with one external cavity diode laser (ECDL) and three acousto-optical modulators (AOM).

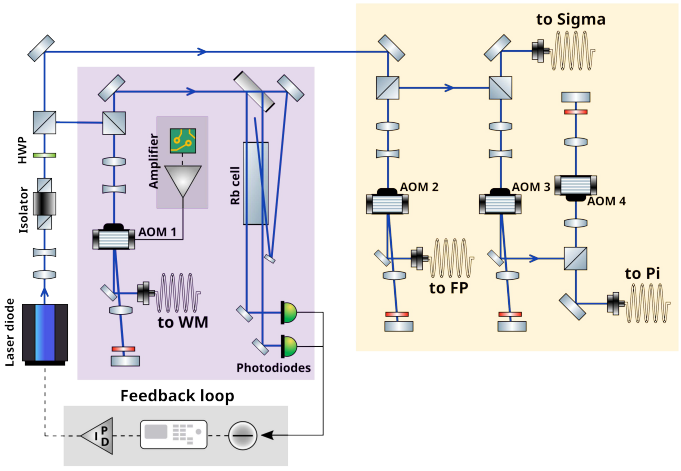

Figure 1: 422 nm laser layout on the optical table.

The laser is frequency stabilized by locking to a nearby transition of rubidium. Rubidium also has a 422 nm transition, $5S_{1/2} \leftrightarrow 6P_{1/2}$, only 440 MHz from the relevant Sr^+ transition. We use saturated absorption to remove the effect of Doppler broadening of the absorption signal. An AOM modulates the frequency of the light that is sent to the Rb vapor cell, and the absorption signal is demodulated with a lock-in amplifier. To implement this locking

scheme, we have created an AOM amplifier capable of modulating RF frequencies. The lock-in amplifier's output provides an antisymmetric signal whose zero crossing is the center of the Rb transition. This output is sent as an error signal to a PID controller, whose correction signal is sent to the current offset of the laser controller.

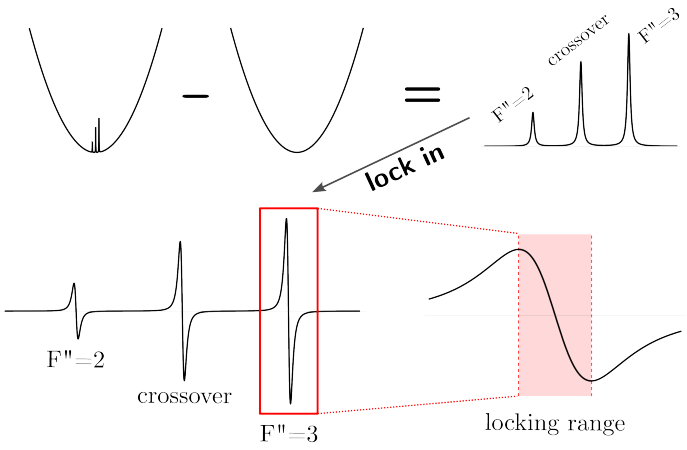

Figure 2: Schematic of signals used to lock the 422 nm laser.

We find that it is possible to lock the laser to an RMS jitter of 30 kHz, which is more than two order of magnitude smaller than the linewidth of the Sr^+ transition. In addition to being a stable laser for probing Sr^+ ions, the laser will also be used to lock other lasers via a Fabry-Perot cavity. The laser, though it can stay locked for minutes at least, may benefit from a simpler feedback loop that takes care of the long-term drift of its frequency.

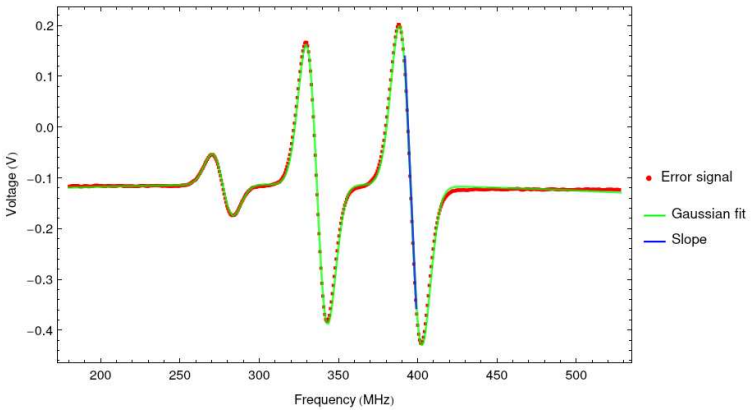

Figure 3: Error signal from the lock-in amplifier.

Acknowledgments

Charlie, I can only imagine how many times you would have (justifiably) wanted to strangle me. Physics has been my dream and I left my country for it — and you're the one that made it possible. I've learned so much and become a better physicist, even if you always say "All I know is how to use a wrench," which I don't believe, since you taught me about screwdrivers too. Thank you for your humor, your guidance, your care. You are a truly amazing teacher, and it was such an honor to learn from you.

Tiku, who is the second reader of this thesis, thank you for your kind and careful advice for this thesis. To you and Professor Tucker-Smith, I am glad I learned quantum mechanics from you. Professor Kealhofer, I think it's safe to say you were my first friend in college. Thank you also for teaching me some really cool physics and for projecting my booming Zoom presence to the class.

Jiwoo, thank you for your humorous and serious ways of love. You've been forced to listen to me in my honest torment too many times, which, in retrospect, is a little embarrassing. I really have never played the 선배 role. Katie, thanks for letting me cry in front of you so many times. You are the most gentle and compassionate friend. You'll have to endure for a few more years my calls of *Krockmeyer*. Bless, thank you for a friendship that I'll never forget. You are one funny man — and I'll miss you a lot. Sonya, I'll always remember the many times you rescued my butt. Too many times, honestly. Charles, Abby, Katya, Justyn, Robin, Jonathan: thank you for an amazing time. It is an honor to know all you kind, hilarious, and brilliant physicists. Benny, you're alright. Just joking — you were my role model and my beer buddy for my first two years. I'll always be grateful for that. Sam, with you in the Doret lab, the future is truly brighter than the past. (Forrest, you too.) You're also so much more than a good physicist; you're a good comrade. To all the students that came to my TA session, thank you for some great memories. Sometimes I went into TA sessions feeling tired and disspirited. I always left happy and joyful. Please remember that I believe that you will all be amazing physicists, even if it's hard sometimes. Devika, thank you for reminding me, again and again, the things that are worth fighting for. I am lucky to have you as a friend. May I never forget the strength and courage you have shown us all. Gaaloo, Angelica, Amelia, Kit, Bemnet, and Ruby — I would never have found my ground at Williams without all of you. You have steadied me when I felt shaken.

Michael, I apologize for all past and future hours of sleep lost as we talk about physics, politics, history, mathematics, and squirrels. Isn't it crazy that we met? How many chaotic

systems swung one way and not others such that we found each other? Thank you for being your gentlest, kindest, and most caring self to the scared and stressed 20-year-old me. Thank you for continuing to be your most patient and loving self to the more obnoxious 22-year-old me. Here's to many more hours of arguing and teasing — I promise I will sometimes shut myself up and just be nice.

My special thanks to mozzarella sticks from 'snar', coffee from Driscoll, and masala chai from Spice Root for filling my sometimes empty heart.

마지막으로, 타국에서 전화도 자주 하지 않는 딸을 늘 응원해주신 사랑하는 부모님과 동생에게 고맙다는 말을 전하고 싶습니다. 걱정 끼쳐드려 죄송하고, 키워주셔서 감사합니다. 저도 제가 정말로 물리 공부를 하는 걸 오래 좋아할 줄은 몰랐는데 말이죠. 이 논문 쓰면서, 엄마 아빠 덕분에 미국에 와서 이런 공부도 마음껏 해본다는 생각을 자주 했어요. 제가 꿈을 이룰 수 있도록 이끌어주셔서 감사합니다. 다형아, 언니가 독립(?)을 조금 일찍 해서 언니 노릇을 많이 못했어. 엄마 아빠랑 혼자 있느라 힘들었지! 이번 여름에는 꼭 붙어있자. 전화할 때마다 기껍게 받아줘서 고마워. 언니가 사랑한다!

빼앗긴 들에서 봄을 기다리는 모두에게 이 논문을 바칩니다.

Contents

List of Figures

Chapter 1

Introduction

Recently, as one possible application of a universal quantum computer, physicists have become interested in *digital* quantum simulations. Simulating the evolution of a quantum system on a classical computer can easily become intractable. Digital quantum simulations offer the possibility of a discrete mapping from the Hamiltonian of the system to a completely different Hamiltonian of another quantum system. This means that observing the evolution of the latter system, which is usually simpler, can reveal something about the time evolution of the former, more complicated system, which would be practically impossible to understand with a classical computer.

The Doret lab is interested in *analog* quantum simulation. Unlike its digital counterpart, analog quantum simulation is often used to 'simulate' the dynamics of a many-body system by using a simpler quantum system whose interactions are capable of emulating similar dynamics to the original system. Here, the mapping between the Hamiltonians are continuous, and more 'obvious'.

The Doret lab has previously pursued precision measurements on Ca^+ ions and is now transitioning to analog quantum simulations of heat flow. This introduction will summarize the new goals and tools of the lab as we make this change.

1.1 Analog simulation of thermal diodes

Thermal rectification refers to the phenomena of asymmetric heat transfer. Consider a metal stick with hot coal on one end, and a bucket of ice in the other. If one observes a different rate of heat flow when the two ends of the metal stick are flipped, then thermal rectification has occurred. A theoretical paper by Simón [1] predicts thermal rectification in two coupled oscillators, each connected two thermal baths of different temperatures. It also asserts that this should be realizable through two trapped ions, and suggests situations in which the rectification would be maximized. The current goal of the lab is to experimentally realize the paper's findings.

An immediate next step to that goal is to have two different species of ions in the same trap. Clearly, there must be some asymmetry in the system to observe heat rectification, and

the most straightforward way to create that asymmetry is to have two coupled oscillators of different masses. Our lab has chosen Strontium ions to be trapped in addition to Calcium.

In the long term, the Doret lab wishes to simulate heat transfer in ion chains. One can imagine a very simple model of a 'crystal' through which heat flows — an N coupled oscillator, where Hooke's Law interactions between adjacent oscillators carry energy through the system. This kind of physics leads to a system whose motion can be decomposed into N different modes of different characteristic frequencies. In the macroscopic world, however, one observes heat flow that is well described by Fourier's Law, which does not describe a ballistic oscillation of heat between two ends of a metal pipe. Then, the question of the mesoscopic regime, between the microscopic regime of ballistic motion and the macroscopic regime, poses an interesting phenomenon.[2]

This goal also requires that we have two different species in our ion trap — one to form the ion chain, and the other to be the thermal bath. The ions that form the thermal bath will have to maintain a constant 'temperature' and thus need constant cooling, while resolved sideband thermometry, which will be explained briefly in Chapter 5, will be applied to the test ions that form the chain. It will thus be important to have a robust setup for trapping and controlling both Ca^+ and Sr^+.

1.1.1 Why EIT?

In the context of trapped ions, 'temperature' refers to the vibrational quantum number of an ion, or if the ion's state is a superposition of different vibrational states, the average of that number. Thus by 'cooling' we mean a process that lowers the vibrational energy of the ion.

The simplest method of cooling ions is Doppler cooling, which the lab has previously used to cool Ca^+ ions. There is a limit to Doppler cooling, which asymptotes as one increases the laser power. In comparison, EIT cooling has the benefit of a faster cooling rate and a lower limit to how much it can cool, given enough laser power. The system we wish to simulate requires that the rate at which we are able to cool ions (used to 'keep' ions at a certain temperature, especially if they are being used as reservoirs) is faster than the rate at which ions thermalize with each other by exchanging phonons. For more details on why the Doret lab requires EIT cooling, see Robichaud [3]. For more details on the theory of EIT cooling, see [4] [5].

1.2 Sr^+ energy levels and lasers

The Doret lab has the lasers to address the necessary transitions of Ca^+. We wish to now be able to address the analogous transitions of Sr^+.

The Doret lab already has lasers for Ca^+: 375nm, 397nm, 423nm, 729nm, 854nm, 866nm.

For two-photon ionization, we need a new 461nm laser to address the $5S_0 \leftrightarrow 5P_1$ transition, after which any blue laser light will be able to excite the atom to the ionization continuum. This is the same process that we use the 423nm and 375nm lasers for Ca^+. We

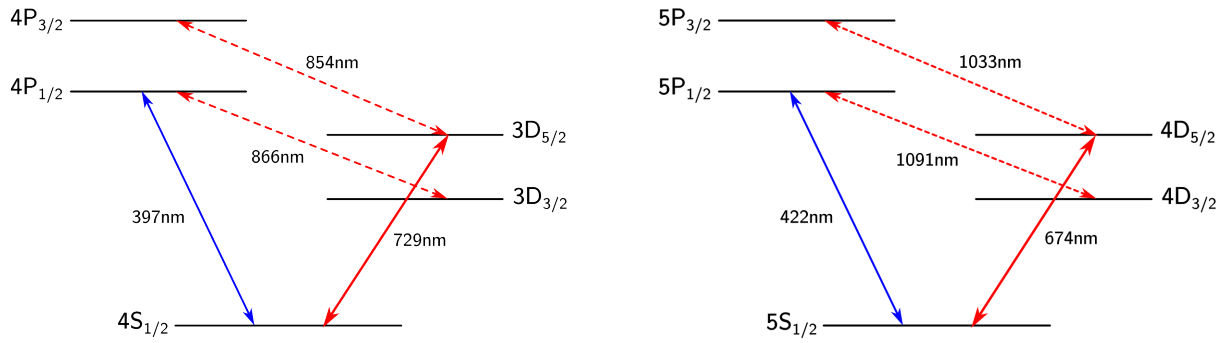

Figure 1.1: Energy levels of $^{40}Ca^{+}$ and $^{88}Sr^{+}$

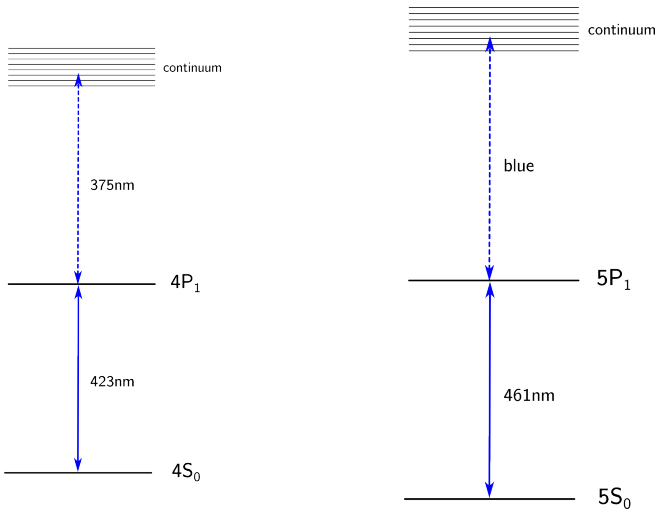

Figure 1.2: Two-photon ionization processes for Ca^{+} and Sr^{+}

need a 422nm laser to address the $5S_{1/2} \leftrightarrow 5P_{1/2}$ transition we use for fluorescence, Doppler cooling, and eventually EIT cooling. This is analogous to the 397nm laser for Ca^+.

We also need 1033nm and 1091 lasers, analogous to 854nm and 866nm, for repumping and quenching. These lasers 'clean out' the ion's state from the metastable D states so that the ions may decay to the ground S state. The 3D states have a natural lifetime on the order of a second, while the 3P states have a lifetime on the scale of nanoseconds. For the time scales of our experiment, a second is as good as infinite. Once the 397nm transition is driven, ions in the $4P_{1/2}$ state can decay to the $3D_{1/2}$ state with a probability of 6.43% [6]. The 866nm transition, when driven, helps return these ions to the ground $4S_{1/2}$ state. And once the 729nm transition is driven, ions in the $3D_{3/2}$ state is returned to the ground state via the higher $4P_{3/2}$ state. From $4P_{3/2}$, the ion can decay to the $4S_{1/2}$, $3D_{5/2}$, or back into $3D_{3/2}$ states; the branching ratios are 93.47:5.87:0.66 [7].

Finally, the analog to the 729nm laser is the new 674nm laser, which is currently in construction. Both of these lasers drive transitions that are dipole-forbidden and electric quadrupole-allowed (E2); thus these lasers must have very narrow linewidth. While our other lasers are homemade external cavity diode lasers (ECDL) with a Littrow configuration, the 729nm laser is a commerical Toptica laser that is frequency-locked with the Pound-Drever-Hall (PDH) method.[8] The 674nm laser will be stabilized by an interference filter instead of a diffraction grating and frequency-locked through PDH. For more details, see Dutton [9].

1.2.1 Frequency stabilizing lasers

All atomic transitions have a natural linewidth, the latter of which is inversely proportional to its natural lifetime. All lasers also have a non-zero spectral linewidth. The Doret lab requires that the laser linewidth is much smaller than the linewidth of the transition, so that scanning over those transitions can produce a faithful representation of the absorption spectrum. The various cooling mechanisms and experiment processes we use also often require the ability to precisely detune laser frequencies. Thus it is important that the laser itself does not have too broad a linewidth. It is also important that the frequency of the laser is stable, since a laser with short-term laser frequency noise has effectively a broadened linewidth, while a laser with long-term noise will simply be incapable of addressing correct transitions.

An additional benefit of having another stable laser is that other lasers may derive their stability from it. Currently, the 397nm, 423nm, 854nm, 866nm lasers are stabilized in a Fabry-Perot cavity with respect to a commercially stabilized HeNe laser. However, as the lab makes more lasers to address Sr^+, it becomes impossible to stabilize all additional lasers in the same Fabry-Perot cavity. Moreover, to lock lasers of a wide range of wavelengths in the same Fabry-Perot cavity can be suboptimal due to their different free spectral ranges (FSR). Thus, it is our hope that the blue lasers will be locked with respect to the newly stabilized 422nm laser, and the redder lasers will be locked with respect to the existing HeNe. For more details, see Bah Awazi [10].

This thesis describes the construction of the 422nm laser for Sr^+. Chapter 2 contains de-

tails of how the laser will be frequency stabilized using saturation absorption on a Rubidium vapor cell, and Chapter 3 will describe the actual implementation of this scheme. Chapter 3 also includes details of the laser path, which generates the necessary frequency shifts and polarizations required by EIT cooling. Finally, Chapter 4 describes the achieved stability of the laser and noises from its components, and Chapter 5 provides the next steps for the Doret lab.

Chapter 2

Laser frequency stabilization scheme

> You know when you get that feeling in your legs, after you've been sitting down for too long? That's what I get, visually, when I look at your blue laser.
>
> Bless Bah Awazi '24

This chapter will describe the frequency stabilization mechanism for the 422 nm laser, which is to lock the laser to a nearby transition of Rb. The natural linewidth of the Sr^+ transition is $2\pi\times20$ MHz.[11] Ideally, the laser that addresses this transition should be stabilized to an order of magnitude smaller than this linewidth, and preferably less.

2.1 Saturated Absorption of Rubidium

The electronic structure of the atom includes hyperfine splittings, which arise from the coupling between nuclear and electronic angular momentums. Thus, this splitting depends on the isotope of the atomic species, because different isotopes have different nuclei, with different nuclear spins. The different F numbers indicate hyperfine levels in Figure 2.1.

One of the Rb transitions between hyperfine structures of Rb manifolds $5S_{1/2} \leftrightarrow 6P_{1/2}$ is only 440 MHz red of the Sr^+ $5S_{1/2} \leftrightarrow 5P_{1/2}$ line, which is the main fluorescence and cooling transition.[12] This fortunate coincidence gives us a relatively straightforward way to lock the frequency of the laser, given the availability of Rb vapor. If one can ensure that the frequency of the laser remains at (or is very close to) the center of the Rb absorption line, then we would have stabilized the laser. (This 440 MHz difference must be offset in the laser path. For more details, see Chapter 4.)

Of course, the transition linewidth of the Rb transition is not infinitely narrow, and the quality of the frequency lock depends on this linewidth. The natural linewidth of the Rb $5S_{1/2} \leftrightarrow 6P_{1/2}$ transition is $2\pi\times$ 240 kHz, which is sufficient to provide a very good lock. In practice, we do not have access to this linewidth without further considerations.

Any gas of atoms at non-zero (Kelvin) temperature has a spread out velocity distribution.

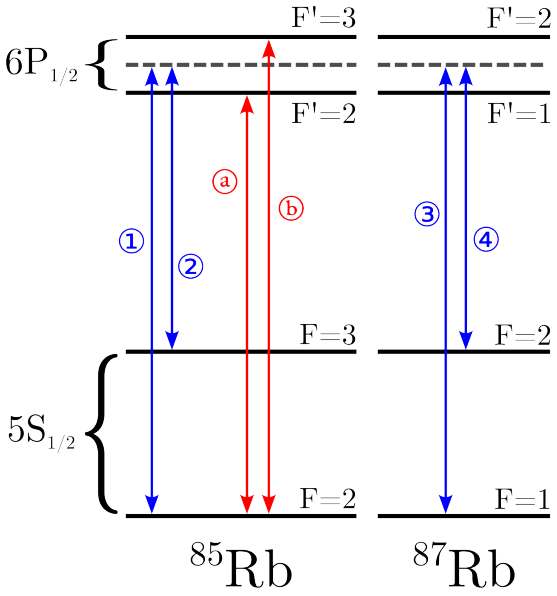

Figure 2.1: Relevant hyperfine structures of ^{85}Rb and ^{87}Rb. Each transition is given a label that reference Figures 2.3 and 2.4. Energy splittings not to scale. Modified from Glaser [13].

The atoms that are moving relative to the laser source 'sees' a different frequency than the frequency of the photon at its source. So, even if the photon is detuned from an atomic transition, there may be some atoms with the right velocity that are able to absorb this photon. This leads to a broadening of the absorption spectrum called Doppler broadening.

Saturated absorption spectroscopy (SAS) is a method to remove this Doppler broadening from the absorption spectrum. Two counterpropagating laser beams of the same frequency are passed through the vapor cell. The frequency of these lasers then can be scanned over the transition to reveal the absorption spectrum.

One of the overlapped, counterpropagating laser beam, called the pump beam, is typically much more powerful than the other, called the probe beam. Suppose at some frequency, both laser beams are resonant with an atom. Then the pump beam *saturates* the transition; the number of atoms in the excited state and in the ground state are roughly equal. When the probe beam reaches the saturated atom, there is a good chance that the atom has already been excited. Thus, there is less absorption when the two beams are at a frequency that is simultaneously resonant with the same atom. Notice that this is only possible with atoms that are moving perpendicular to both the pump and probe beam, since they are the only atoms that do not 'see' Doppler shifted frequencies. If an atom is moving towards the source of the pump or probe beam, the frequency that the atom 'sees' will be different due to the Doppler shift. In this case, the probe beam is absorbed by the same amount regardless of the pump beam. The net effect of saturated absorption spectroscopy is that there is less absorption when the frequency of the laser is resonant with the zero velocity class atoms,

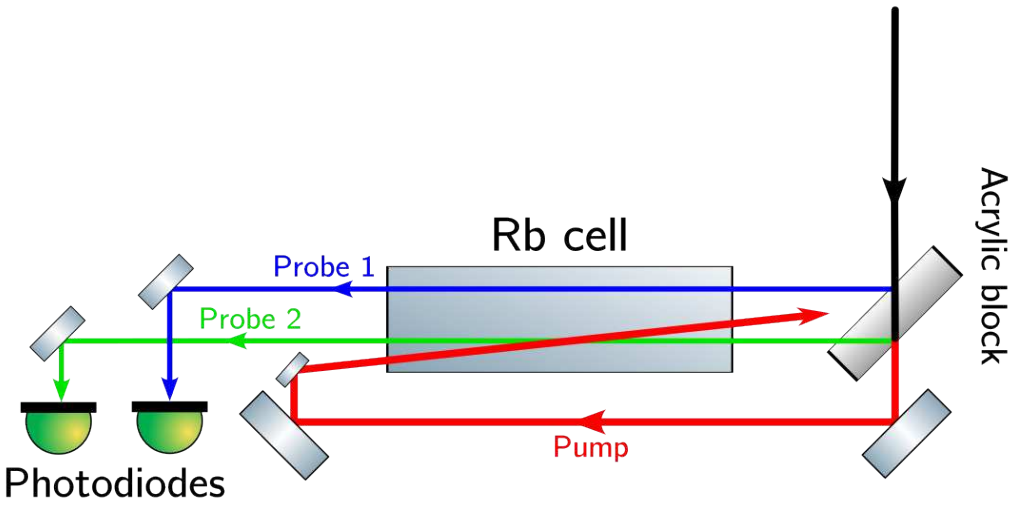

Figure 2.2: A setup for saturation absorption spectroscopy.The acrylic block lets most of the light through, which makes the pump beam (in red). The two beams reflected from the surfaces of the block make the two probe beams (in green and blue) which are later subtracted from one another to remove the Doppler-broadened absorption profile. The green probe, labelled Probe 2, contains the Lamb dips from saturated absorption.

and this 'peak' is no longer subject to Doppler broadening.

It is this narrow peak that we lock our laser to. One should note that if there are multiple absorption lines close to each other, we observe crossover peaks in our SAS spectrum. These occur at the midpoint between two transitions, and are caused by a lack of absorption in the group of atoms that are not moving quite perpendicular to the pump and probe beams. These atoms move in just the right velocity such that the pump beam saturates one of the transitions, which cause the probe beam to be transparent to these atoms. If the atom's electronic structure has hyperfine levels close to each other, then there will likely be a crossover peak halfway between the two hyperfine peaks.

2.1.1 Transition strength and vapor pressure

It should be noted that the most common transition of Rb used for spectroscopy (for example, in PHYS 301) is the 780 nm transiton between $5S_{1/2} \leftrightarrow 5P_{3/2}$, which is much stronger 422 nm transition. The natural linewidth (also Einstein A coefficients) of the 780 nm transition is $2\pi\times$ 6 MHz, while that of the 422nm transition is $2\pi\times$ 240 kHz.[11] Note the ω^3 dependence in the linewidth [14]:

$$A_{21} = \frac{g_1}{g_2}\frac{4\alpha}{3c^2} \times \omega^3 |D_{12}|^2, \tag{2.1}$$

where g_1 and g_2 are the degeneracies of each energy level, α is the fine structure constant, c is the speed of light, and D_{12} is the reduced matrix element.

We know that SAS on the Rb transition at 780 nm is straightforward. In comparison, how much harder is SAS for the 422 nm transition? In terms of the dipole moment matrix element, $eD_{12} = \langle\psi_1|e\vec{\mathbf{r}}|\psi_2\rangle$, which describes the strength of the transition, $|D_{780}|^2$ is about 160 times larger than $|D_{422}|^2$.

This characterizes how coupled the two electronic states are, but is not a direct description of absorption. In terms of absorption, we consider that

$$\frac{dI}{dz} = -N\sigma(\omega)I \tag{2.2}$$

where N is the number atoms per volume, I the intensity of light after passing through a length z of the absorptive medium, and $\sigma(\omega)$ is the absorption cross-section. The absorption cross-section near resonant frequency ω_0, as a function of the optical frequency, is

$$\sigma(\omega) \sim \frac{A_{ki}}{\omega_0^2}\frac{\Gamma}{(\omega-\omega_0)^2+\Gamma^2/4}, \tag{2.3}$$

up to a multiplicative constant, where $A_{ki} = \Gamma = \tau^{-1}$ is the natural linewidth and the inverse of the lifetime [14]. At the resonant frequency, $\omega = \omega_0$, Γ cancels out, and the absorption cross-section is simply proportional to the square of the wavelength. Thus, $\sigma(780\text{ nm})$ is about 3.4 times larger than $\sigma(422\text{ nm})$.

For this blue transition to exhibit comparable absorption to the 780 nm transition, we heat the Rb vapor cell to at least 80°C, and usually above 90°C. ([12] heats the Rb vapor cell to 100°C.) Some back-of-the envelope calculations may be useful to motivate the heating of the vapor cell. The Clausius-Clapeyron equation (or the approximation thereof) describes the temperature dependence on the vapor pressure of some material whose gaseous form follows the ideal gas law, along with other assumptions, such as a constant latent heat for different temperature/pressure conditions, and a much smaller volume of solid or liquid than there is of gas.

$$P_{vapor} = P_0 e^{-L/RT} \tag{2.4}$$

Here, P_0 is some constant with a dimension of pressure, R is the molar gas constant, and L is the latent heat needed for transitioning into the gaseous phase, which we have assumed to be constant across the temperature range we are interested in.

We can imagine our Rb vapor cell as a tiny amount of solid or liquid in vacuum to start. (Under atmospheric pressure, at 40°C, Rb transitions from solid to liquid.) Rubidium will partially evaporate or sublimate into gas, until the gas reaches the vapor pressure for the temperature of the vapor cell. The Clausius-Clapeyron equation tells us that this vapor pressure scales with $\exp\{-L/RT\}$. The number of gaseous atoms in the vapor cell, then, scales as $\frac{1}{T}\exp\{-L/RT\}$. Thus, given a limited optical absorption cross-section in the 422 nm transition, we increase the N in Equation 2.2 by heating the vapor cell. Pandey [15] finds 84°C to be optimal. A thermistor on the vapor cell allows us to monitor the vapor cell's temperature.

Finally, we note the saturation intensity of our transition [14],

$$I_{sat} = \frac{\pi}{3}\frac{hc\Gamma}{\lambda^3}$$

is roughly $4\mu\text{W/mm}^2$. This is the laser intensity at which the atoms are equally likely to be in the excited and ground state, and the intensity that we need the probe beam's intensity to exceed in order to have the strongest Doppler-free peaks, which is not very difficult. In order to guarantee that the probe beams do not saturate the transition, as the pump beam does, we also need the probe beams to be weaker than this intensity, which make require more care. A probe beam that is too powerful will not only decrease the contrast of the absorption, but also cause power broadening, where the lifetime of the upper state is reduced due to stimulated emission in the presence of a strong resonant light.

2.2 Observed Rb spectra and peak identification

While the laser path includes a wavemeter that measures the frequency of the light out of the laser diode, this is not sufficient for identifying peaks on its own. First, the wavemeter has not been calibrated for a while, and due to a broken component we cannot calibrate it without checking the fluorescence from a trapped ion. Thus, whereas we do know relative frequency differences, we cannot quite trust the wavemeter's absolute frequency.[1] Second, the wavemeter's output precision, even when calibrated, is only 100 MHz. This means that one can use the wavemeter to crudely measure the hyperfine splitting in the $5S_{1/2}$ manifold, which have somewhat resolved absorption peaks even with Doppler broadening, but not for the hyperfine splitting in the $6P_{1/2}$ manifold.

For identifying all the absorption peaks, we use literature values from [13].

2.2.1 Doppler-broadened spectrum

Figure 2.3 shows the Doppler-broadened spectrum of Rubidium, taken from an oscilloscope trace of a photodiode signal while the laser's frequency is scanned through its controller, and while there is no pump beam to saturate the transitions. The hyperfine splitting of the $5S_{1/2}$ manifold is much larger than that of the $6S_{1/2}$ manifold. The Doppler-broadened width of the peaks is of order 1 GHz. This means that the hyperfine splitting of the $5S_{1/2}$ states are mostly resolved, while the $6S_{1/2}$ splitting is not visible from this spectrum.

The natural abundance of Rb consists of 72.2% ^{85}Rb and 27.8% ^{87}Rb, which means there is more absorption at ^{85}Rb transitions. For Table 2.1, we record wavemeter values where the photodiode's output voltage is at a minimum.

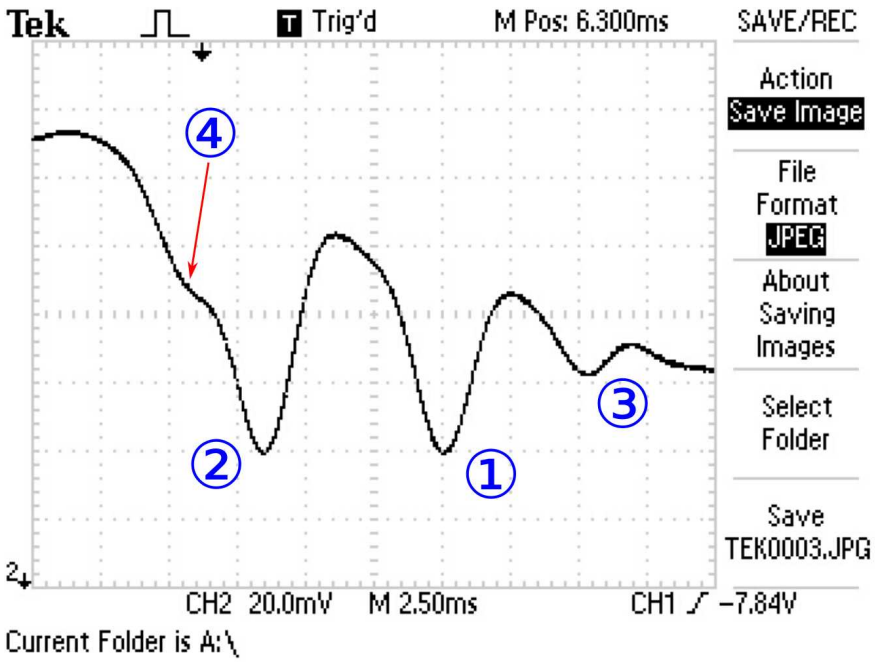

Figure 2.3: Doppler-broadened Rubidium spectrum. Labels reference the hyperfine level structure in Figure 2.1.

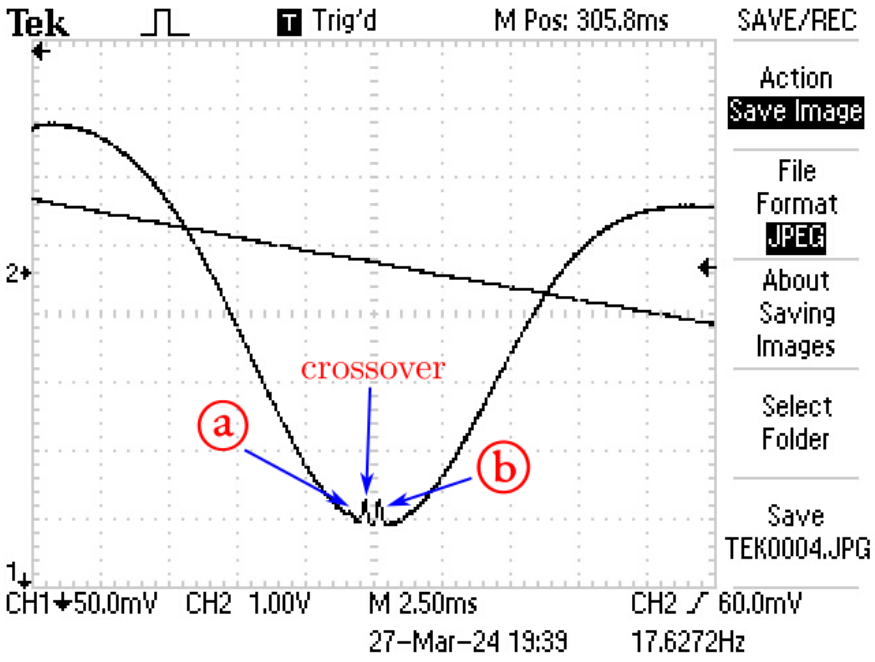

Figure 2.4: Doppler-free Rubidium spectrum. Labels reference the hyperfine level structure in Figure 2.1.

Species	F	Fig. 2.1 label	Wavemeter - 440 MHz (THz)	Literature (THz)
^{87}Rb	2	④	N/A	710.9581
^{85}Rb	3	②	710.9591	710.9593
^{85}Rb	2	①	710.9622	710.9623
^{87}Rb	1	③	710.9648	710.9649

Table 2.1: The local minima of the Doppler-broadened signal, Figure 2.3.

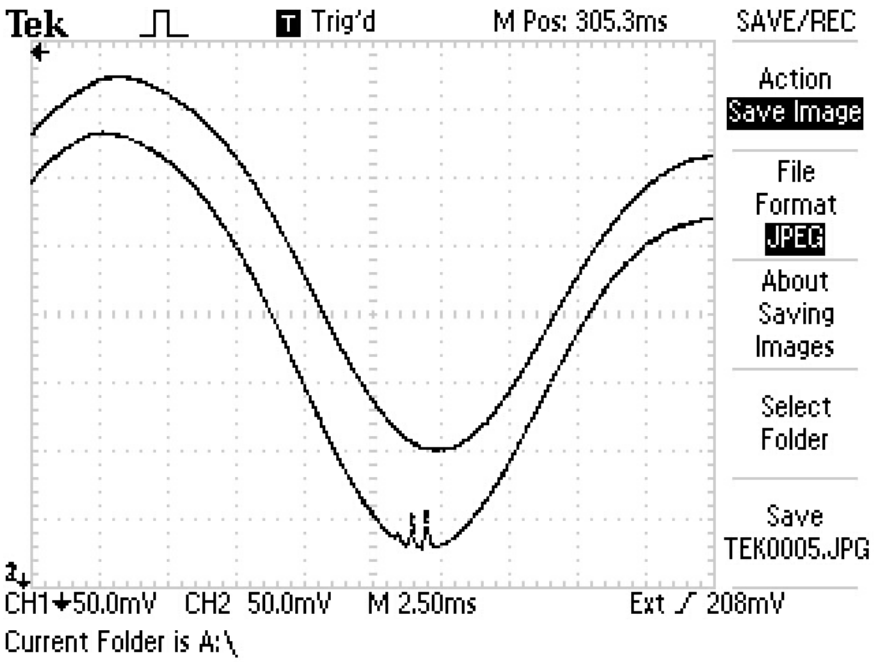

Figure 2.5: Doppler-free and Doppler-broadened spectra, from the two different photodiodes. The signals are then subtracted by the lock-in amplifier.

2.2.2 Doppler-free spectrum

In his master's thesis, Shiner [12] locks his laser to the Rb transition $5S_{1/2}$ (F=2) $\leftrightarrow$ $6P_{1/2}$ (F=3), labeled ⓑ in Figure 2.1. The Rb transition is only 440 MHz away from the Sr^+ transition. From this number and the spectrum from [13], we find that the hyperfine level that Shiner used is indeed the closest one to the center of the Sr^+ line. Therefore, we lock to this transition since it is within range of frequency shifts that can be provided by our AOMs.

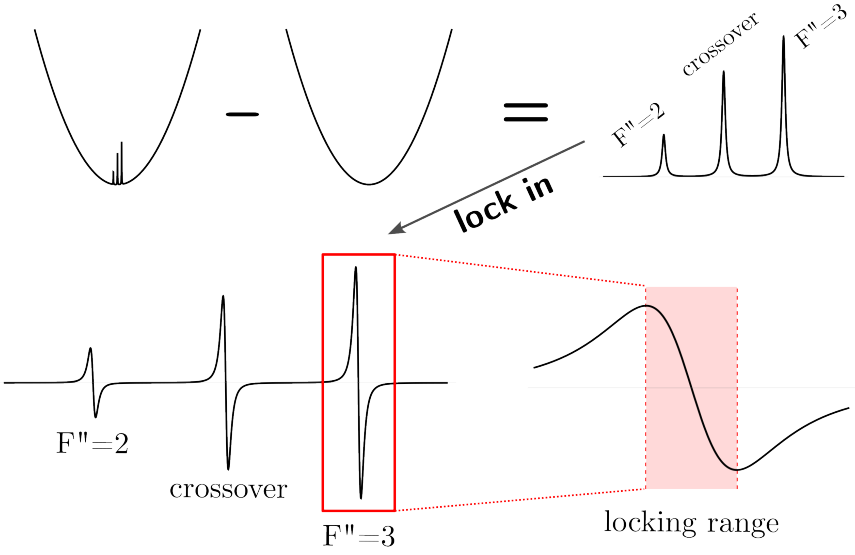

Figure 2.6: Schematic of signals in locking the 422 nm laser.

2.3 Lock-in detection

Once we find the Doppler-free peak of $5S_{1/2}$ (F=2) $\leftrightarrow$ $6P_{1/2}$ (F'=3), we need to be able to lock to the center of this peak. The photodiode, at a given time, outputs one value; from this value we must be able to tell whether the laser is red or blue of the transition so that we may send a correction signal of the correct polarity. The Doppler-free peak is symmetric with respect to the center of the transition; it cannot provide the adequate error signal. We thus use lock-in detection to generate an anti-symmetric signal.

By modulating the signal by a known frequency (using an AOM and a homemade amplifier, explained in detail in Chapter 3) and demodulating it at that frequency with a lock-in amplifier, we effectively differentiate the Doppler-free peak. [16] The amplitude of this modulation should be much smaller than the width of the spectrum's feature itself to achieve this differentiation. This signal, then, is odd and has a zero-crossing exactly at the center of the peak, at least in the range marked red in Figure 2.6. This is exactly the anti-symmetric signal that we need.

In practice, the error signal is not always centered at 0V. This can mean, for example, to actually lock to the center of the transition, we may need to set the laser's feedback to lock to an offset. (The offset has usually been on the order of 50–150 mV.) To create Doppler-free peaks, we subtract two Doppler-broadened signals — one with Lamb dips, and one without. We use a variable ND filter wheel to balance the intensity of the signals. This subtraction is usually imperfect due to nonlinearities in the photodiode circuit or imperfections in the optical path. This can lead to an overall slope to the Doppler-free spectrum. This slope is

[1]We have reason to believe that it is accurate up to 1 GHz.

exacerbated when the Lamb dips are not at the center of the Doppler-broadened dip due to imperfect optics misalignment.

A lock-in amplifier also requires a time constant to be set. It is, roughly speaking, the time for which the input signal multiplied with the reference signal is integrated, a 'projection' in the Fourier space. Equivalently, it is also the inverse of the cutoff frequency for a low-pass filter that operates on the multiplied input and reference signal. A time constant that is too short will be subject to high frequency noise, while a time constant that is too long may slow down the feedback in locking the laser. Since we modulate the AOM by roughly 15–45 kHz, we have found 100–300μs to be adequate as the time constant.

Finally, the greatest advantage of lock-in detection is that it significantly improves signal-to-noise ratio (SNR), which is why it is frequently employed with saturation absorption spectroscopy. By selecting only signals at the reference frequency, it makes the experiment much more robust to transient noises.

2.3.1 PID feedback

A PID circuit is a simple feedback loop that is agnostic to the working of the device under test (DUT). All it needs is a signed error signal such that a negative signal and positive signal mean errors in the opposite direction. Often, the zero-crossing of the signal is the lock point, so that the PID circuit will try to make the error signal as close to zero as possible. It generates a correction signal that somehow affects the DUT, but it does not need to know how the DUT functions in response to that correction signal. (In contrast, the feedforward in the laser controller circuitry must be tuned ahead of time with the knowledge of how the cavity mode hops in response to increasing the PZT voltage, and how the laser diode responds to an increased current.) The laser controller also stabilizes the temperature of the laser diode using a similar PID circuit.

Suppose that the error signal is $\varepsilon(t)$. In our experiment, this would be the output signal from the lock-in, subtracted by the lock's setpoint, the 'goal' that the PID tries to achieve. Then the correction signal sent to the laser is,

$$\text{correction}(t) = P \cdot \varepsilon(t) + I \cdot \int \varepsilon(\tau) d\tau + D \cdot \frac{d\varepsilon(t)}{dt},$$

where P, I, and D are proportional, integral, and derivative coefficients, respectively, that must be tuned.[2] P corrects proportional to the absolute size of the error; I corrects for accumulated errors over a long period of time, and D corrects any persistent oscillatory

[2]While this is the standard definition of what the P, I, and D coefficients do, note that the commerical PID controller currently in use in the lab defines its coefficients differently. There, it is

$$\text{correction}(t) = P \cdot \left\{ \varepsilon(t) + I \cdot \int \varepsilon(\tau) d\tau + D \cdot \frac{d\varepsilon(t)}{dt} \right\},$$

which means that the actual integral and differentiation coefficients are coupled with the changes in P coefficient as well.

behavior. Most importantly, without the correct polarity of the P coefficient, one will in fact push the laser away from the lock point. Though it takes some trial-and-error, monitoring the wavemeter and the error signal while changing the polarity of P can determine the correct one.

One sure way of verifying that the laser can be locked is to modulate the laser's frequency through the PZT offset. Though this may seem counterproductive, if the laser is subject to a well-controlled 'noise' (such as a slow sawtooth wave), one should be able to see that the correction signal is also roughly a sawtooth wave, since it tries to counteract the effect of the sawtooth signal. When the signal to the PZT offset is turned off, the laser frequency should remain relatively stable in the wavemeter's frequency graph.

Chapter 3

Laser implementation

In this chapter, we implement the stabilization scheme described in Chapter 3, and make the path of the laser appropriate for EIT cooling. Many of the same techniques and designs used for previous lasers are also used here. The details most specific to the 422 nm laser is the frequency-modulated RF signal sent to an AOM, and the frequency shifts that the AOMs are designed to implement.

3.1 422 nm laser

The external cavidy diode laser (ECDL) and the laser controller used for the 422 nm is of the same design that has been used for the other Ca^+ lasers that address dipole-allowed transitions, such as 397 nm. We use a Nichia NDV4A16E diode, whose stated maximum output power is 120 mW, more than sufficient for our purpose. Note that we use a laser controller with a 'negative' current source, as a result of the laser diode's polarity. The controller is also constructed such that a decrease in PZT voltage corresponds to an increase in frequency, at least in the same lasing mode. See Appendix C for more details on laser diode polarity.

3.1.1 Laser path diagram

The laser's layout and its actual setup on the optical table is described in Figure 3.2. The beam is first collimated with cylindrical lenses, and then there is an isolator to prevent optical feedback. The next half waveplate and the polarizing beamsplitter divide the intensity of the light into two parts: one locks the laser, and the other shifts laser frequencies appropriately for EIT cooling.2

The double-passed AOM and the cat's eye retroreflector is a configuration that the Doret lab has employed many times before. AOMs, in a nutshell, are an optomechanical element that takes a radiofrequency signal (typically at tens to hundreds of MHz) and shift a laser beam's frequency by that amount. One can either up-shift or down-shift the frequency of

the light. In doing this, it also diffracts the laser beam by a small amount, and there are usually multiple order of diffraction.

The double-pass configuration allows the propagation direction of the output beam, whose frequency has been shifted by the AOM, to be independent of the frequency shift itself. The cat's eye retroreflector (which consists of a lens and a mirror) is less sensitive to the angle of incidence than a single mirror [17], and ideally, the beam whose light has been shifted by the AOM will not change direction or position even if the AOM's radiofrequency changes. [18] See Figure 3.1. This is particularly important for this setup because in at least three of the AOMs, we will need the ability to change the frequency of the signals sent to the AOM to correctly address atomic transitions; indeed, in one of them, the frequency will be constantly modulated. We typically achieve around ∼80% single-pass efficiency, and ∼60% double-pass efficiency. Note also that since the light passes through the AOM twice, if the AOM receive an RF signal of ΔF frequency, the frequency of the laser beam will be shifted by $2\Delta F$.

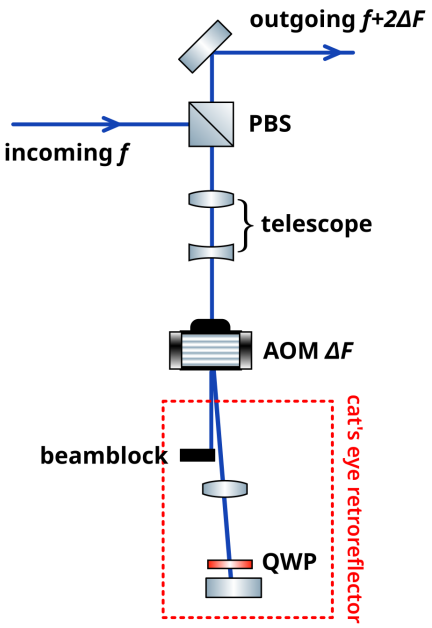

Figure 3.1: The double-pass AOM layout.

The locking mechanism uses AOM 1 in Figure 3.2 to 'dither' (or, frequency modulate) the laser's frequency. The RF amplifier used to achieve this frequency modulation is explained later in this chapter. That dithered light is sent to a Rb vapor cell for saturated absorption, whose Doppler-free peak will be used to lock the laser with a lock-in amplifier and a PID circuit.

The second part of the layout, which appropriately shifts the laser frequencies, consist of three double-pass AOM setups. Notice that AOM 2 shifts the light that both AOM 3 and 4 receive, but AOM 3 does not shift the light that AOM 4 receives. In fact, AOM 4 receives only a small amount of laser intensity unless AOM 3 is off, because the light going into AOM 4 is the zeroth order diffracted beam from AOM 3. The frequency-shifted output from AOM 3 is coupled into fiber, and will be sent to the ion trap to be the σ^- polarized beam. The frequency-shifted output from AOM 4 will also be sent to the ion trap to be the π polarized beam. By adjusting the RF signals sent to AOMs 3 and 4, the relative detunings of these two beams can be accurately adjusted.

Since the AOMs necessarily throw away some light at its zeroth order diffraction, this light is are often coupled to be used elsewhere. In particular, the 'throwaway' light from AOM 1 is sent to the wavemeter, which is capable of roughly telling us the frequency of the laser, and the leftover light from AOM 2 will be sent to a Fabry-Perot cavity. Since

the zeroth order diffracted beams are unshifted by the AOM, both the wavemeter and the Fabry-Perot cavity receives light of the baser laser frequency.

3.1.2 Frequency shifts

We have designed the laser to use three AOMs (labeled AOM 2, 3, 4 in 3.2) to create two lasers of desired frequency. The other AOM, as has already been described, deals with the 440 MHz difference between relevant Rb and Sr^+ transitions, as well as modulation for lock-in detection. See 3.4.

The laser diode lases at a frequency near 710.7627 THz, which is near the Sr^+ transition. Because of the precision and calibration of our wavemeter, it may read 710.7626 THz as well, at least prior to locking. AOM 2 down shifts the laser by 400 MHz, a number chosen because 200 MHz is near of the AOM's peak performance RF, while AOMs 3 and 4 up shift the laser up. We choose this 'down-and-up' shifting in order to be able to control the detuning between the π and σ^- polarized beams while still operating the AOMs near the RF they were engineered for.

3.2 Amplifier box

For the lock-in detection that effectively differentiates the error signal, we need to modulate the signal by a known frequency. To do this, we modulate the frequency of the laser light that is sent to the Rb vapor cell for saturation absorption. Since dithering the frequency at the laser diode is not an option — as that is the very thing we are trying to stabilize — we instead modulate the RF signal that we send to the AOM (labeled AOM 1 in Figure 3.4).[1]

3.2.1 Components of the amplifier box

The amplifier box needs to be able to send an RF signal whose modulated frequency is centered at 220 MHz. To this end, its main components are a seed oscillator circuit, a voltage controlled oscillator (VCO) Mini-Circuits ZOS-300+, and an RF amplifier ZHL-1-2W-S+. The seed oscillator circuit contains a relaxation oscillator with adjustable resistors, which creates a signal (see Figure 3.8a) that goes to the VCO, and another signal (see Figure 3.8b). (See also Figure 3.7 and Appendix B.) A VCO is a component that creates a sinusoidal oscillation whose frequency is linear to its input voltage. If it receives a DC voltage, it would output a simple sinusoid of one frequency. So, if the VCO receives an oscillating signal, it outputs a frequency-modulated signal — an oscillation whose frequency oscillates. The RF amplifier then amplifies this signal by +24 dBm. AOM 1 can take to approximately ∼25 dBm of power, but we send a signal of ∼17 dBm of power. The box currently has attenuators that take its power down; we can send more power as necessary.

[1] Others have chosen to dither the center of the Rb transition itself using a changing magnetic field; however, we choose to not modulate the line from which the laser locks to and derives its stability.

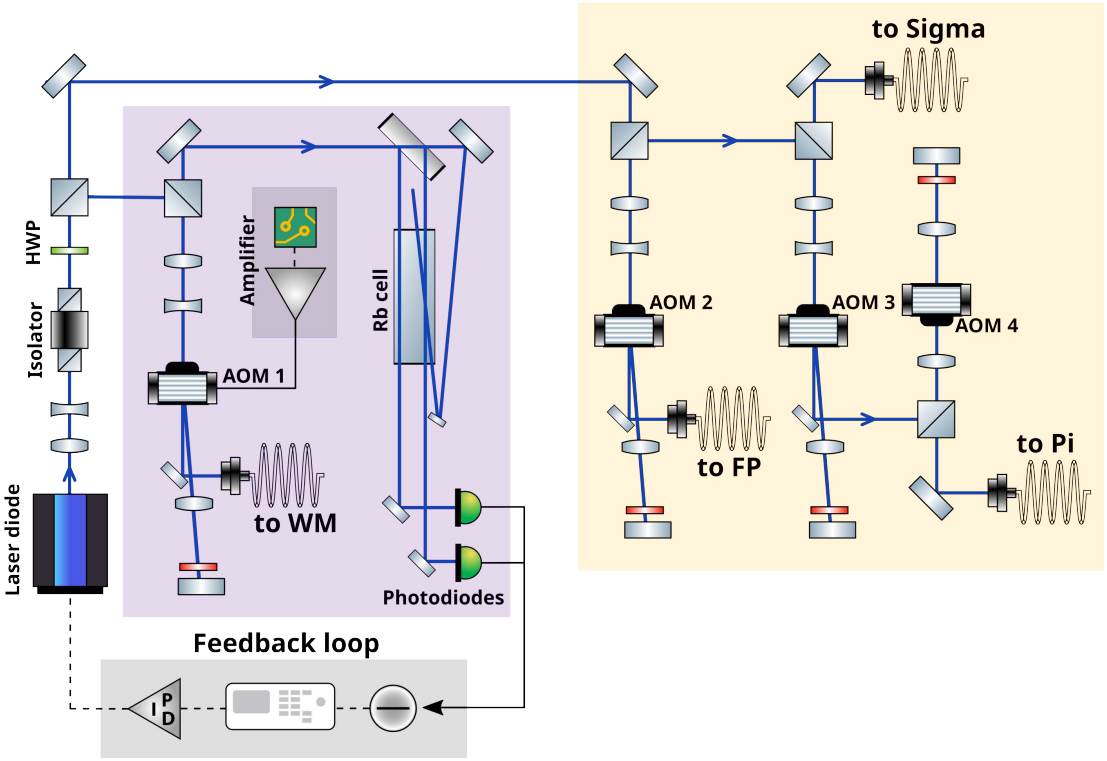

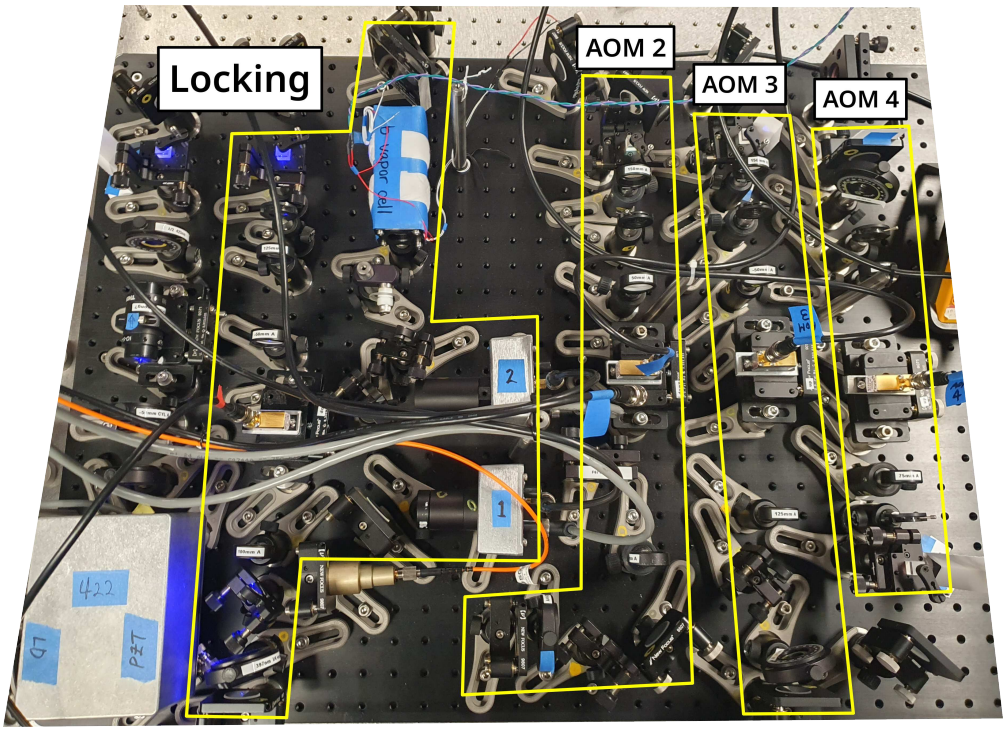

Figure 3.2: 422 nm laser on the optical table and its layout.

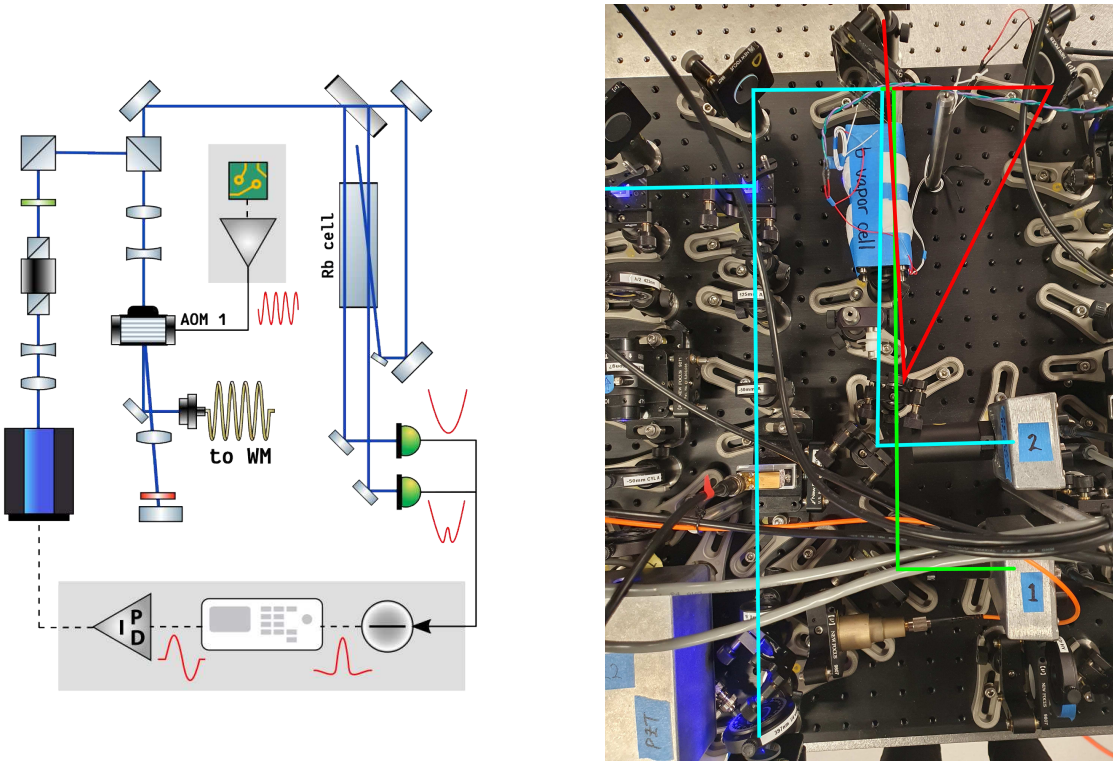

(a) The locking mechanism layout. (b) The locking mechanism on the optical table.

Figure 3.3: The optics and optomechanics used for locking the laser. The Rb vapor cell is slightly tilted to minimize retroreflection from the vapor cell windows being detected by photodiodes.

Though it is not strictly necessary (but helpful for tuning), the box has the ability to change the center frequency f_0, the amplitude of the frequency modulation Δf, and the frequency of the frequency modulation f_{mod} In other words, the instantaneous frequency of the RF signal sent to the AOM would vary between $f_0 - \Delta f$ and $f_0 + \Delta f$, with frequency f_{mod}.

3.2.2 Spectrum

Once we finish assembling the components of the amplifier box, how do we check that the amplifier works as expected? The spectrum analyzer (Agilent 8590L) of the lab is able to take the spectra of RF signals up to 30 dBm in power.

The spectrum we expect is not unlike the spectrum of a FM radio signal, a question that radio engineers care about. [19] Suppose we have center frequency $f_0 = \omega_0/2\pi$, modulation amplitude $\Delta f = \Delta\omega/2\pi$, and modulation frequency $f_{mod} = \omega_{mod}/2\pi$. Then, the signal's instantaneous angular frequency would be

$$\omega(t) = 2\pi f(t) = \omega_0 + \Delta\omega \cos(\omega_{mod} t).$$

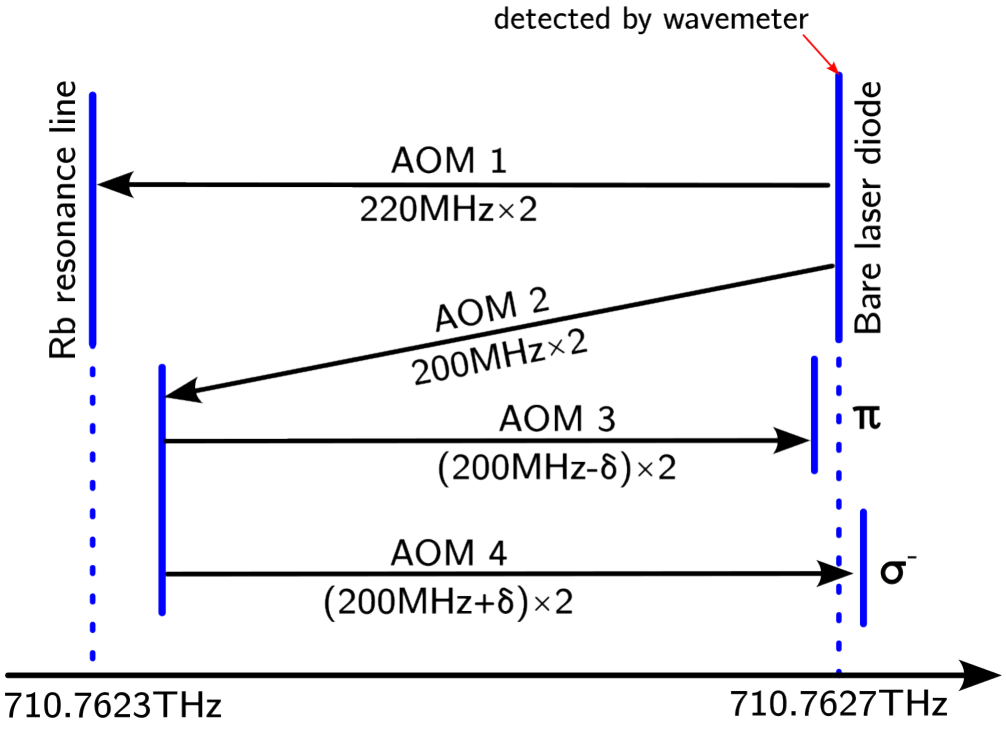

Figure 3.4: Frequency shifts caused by the four AOMs.

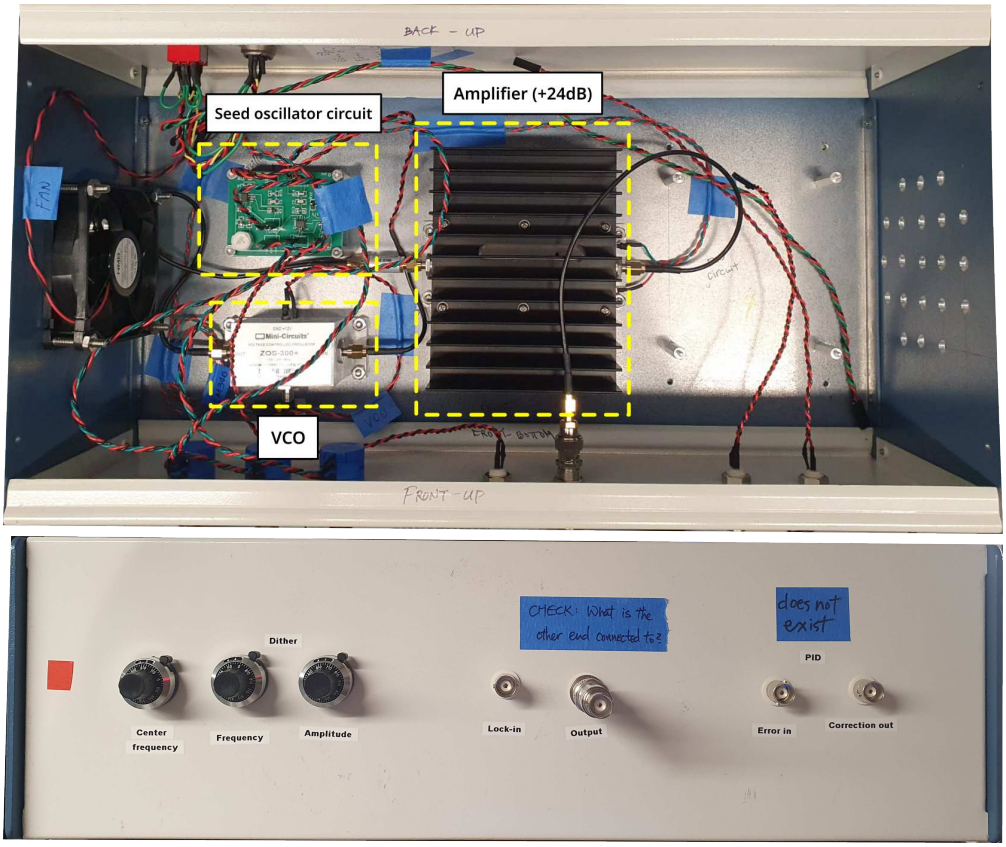

Figure 3.5: Inside and front of the amplifier box.

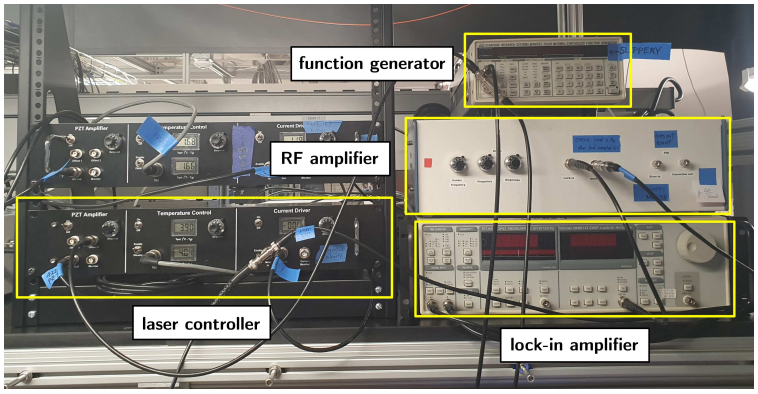

Figure 3.6: Devices used to control the 422 nm laser system. Not shown here are the DC voltage supply that heats the Rb vapor cell, which is behind the RF amplifier, and the PID controller, which is under the other optical table.

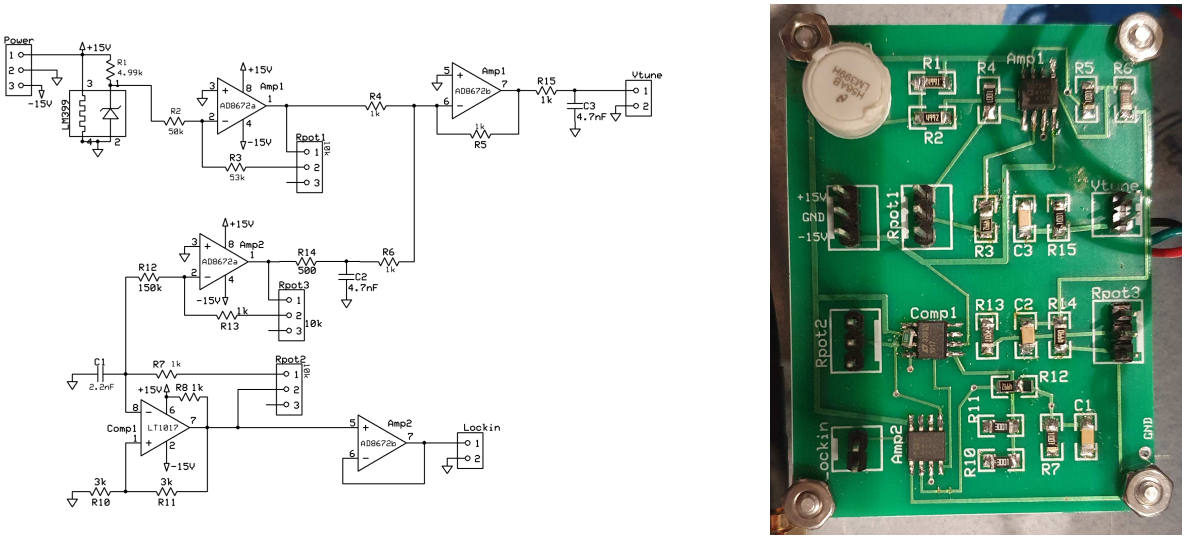

Figure 3.7: Schematic and picture of the seed oscillator.

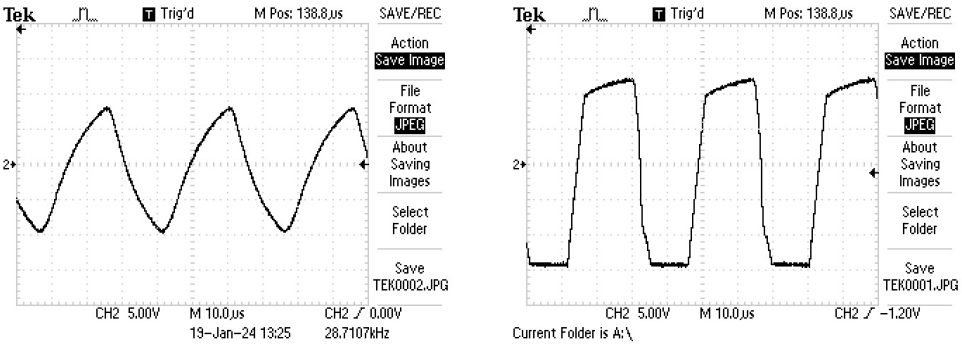

(a) For the VCO. (b) For the lock-in reference.

Figure 3.8: Signals from the seed oscillation circuit.

Since phase is an integral of angular frequency, we express the signal as

$$\text{signal}(t) = \cos\left[\int_0^t \omega(\tau)d\tau\right] = \cos[\omega_0 t + \beta\sin(\omega_{mod}t)],$$

where we have defined the *modulation index* $\beta = \Delta f/f_{mod}$. With some trigonometric identities and the Jacobi-Anger expansion, the above becomes

$$\text{signal}(t) = \sum_{n=-\infty}^{\infty} J_n(\beta)\cos[(\omega_0 + n\cdot\omega_{mod})t],$$

where $J_n(x)$ is the nth Bessel function of the first kind, and $J_{-n}(\beta) = (-1)^n J_n(\beta)$.

This gives us an expected RF spectrum from the AOM amplifier. It tells us that at frequencies at integer n number of ω_{mod} away from the center frequency, the amplitude of the signal at that frequency is $J_n(\beta)$. Carson's bandwidth rule also states that most of the power of the frequency-modulated signal lies within a bandwidth of $2f_{mod}(1+\beta)$. With our seed oscillator circuit, our β can range from 65 to 2385.

In making these measurements, we find that the VCO acts slightly different from the manual of ZOS-300+ (or, the manual does not provide sufficient precision). For the signal to be centered at 220 MHz, the monitor output (of the oscillation sent to the VCO) should be centered at 8.79V. Assuming that the VCO's response is linear, we have found $y = 11.1594x + 122.31884$ to provide a good estimate, where x the input voltage, and y is the VCO's frequency in MHz.

We note that this spectrum, nor its modulation index, is not relevant for the actual interaction between light and the Rb atoms. The modulation index is exceptionally high because the modulation frequency, ω_{mod}, is very slow compared to the carrier frequency, f_0. Thus, for the short amount of time that a group of Rb atoms interact with the modulated light, it does not in fact go through the oscillation of frequency ω_{mod}. It only sees a part of that oscillation. These spectra are simply tools to verify that the homemade RF amplifier box functions as expected.

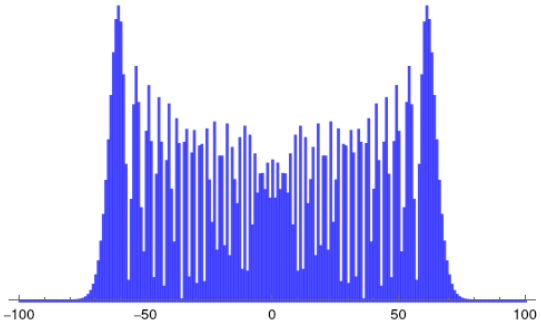

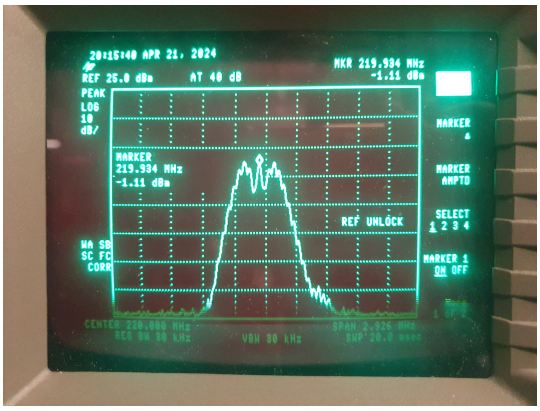

(a) $\beta = 64.24$. Centered at 220 MHz, spans 2.926 MHz.

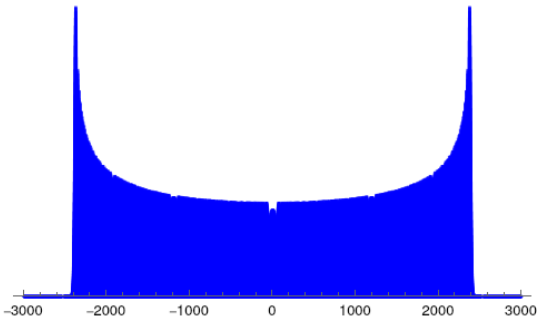

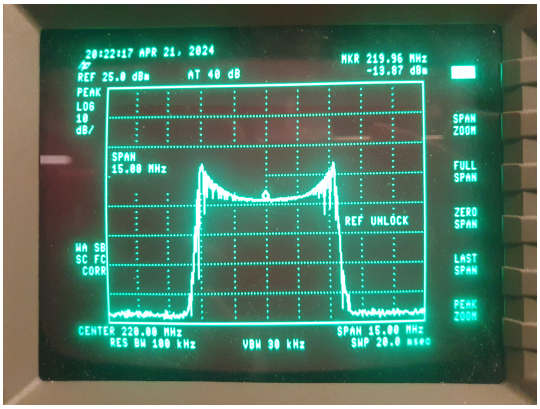

(b) $\beta = 2385$. Centered at 220 MHz, spans 15 MHz.

Figure 3.9: Predicted and measured RF spectra of the amplifier box. The predictions assume a sinusoidal modulation, while the relaxation oscillator creates a sawtooth wave. This leads to some discrepancies between the prediction and measurement. Most of the bandwidth, according to Carson's rule, lies bewteen $2f_{mod}\beta$.

Chapter 4

Results

We believe that we have locked the laser to an root mean square (RMS) jitter of ∼30 kHz, which is much better than the stability of the Ca^+ laser for the analogous transition at 397 nm which jitters at around 2 MHz. This instability is too small for the wavemeter to be able to characterize it, since the wavemeter itself fluctuates more than this. The characterization therefore requires carefully analyzing the error signal. In this chapter, we analyze the error signal once the laser is locked using methods of the previous chapter.

4.1 Error signal

When we scan the laser's frequency with a function generated connected to the PZT offset, without turning the PID controller on, we see a signal that looks like Figure 4.1, which looks as we expect from Figure 2.6. We fit either derivatives of Lorentzians or derivatives of Gaussians to this signal to ascertain the center and width of each feature along with the overall offset from zero. From literature values from Glaser et al.[13], we know that the three centers of each derivative-of-Gaussian features should correspond to these frequencies: 710.962 THz added to 276.73 MHz, 336.12 MHz, and 395.20 MHz. By fitting a quadratic polynomial to the relation between time (as measured on the oscilloscope) and literature transition frequency, we can now calibrate the horizontal axis in frequency, a much more useful unit. We expect this relationship to be mostly linear, since we send a sawtooth wave to the PZT offset. However, there may be small nonlinearities in this mechanical oscillation, which is why we have fitted the conversion between time and frequency with a quadratic polynomial. We usually scan the PZT at a rate of 15 Hz.

We find that the with of the features are ∼7 MHz. This is much larger than the 240 kHz natural linewidth, which indicates that there is broadening beyond the natural broadening. We also find that fitting the derivative of Gaussians provide a much better fit than fitting the derivatives of Lorentzians, which indicate a significant inhomogeneous broadening. This suggests that Doppler broadening in the direction *orthogonal* to the pump beam is significant. Other sources of broadening that one might expect is significant in the heated Rb vapor cell, such as power broadening and collisional broadening, are homogeneous and should have

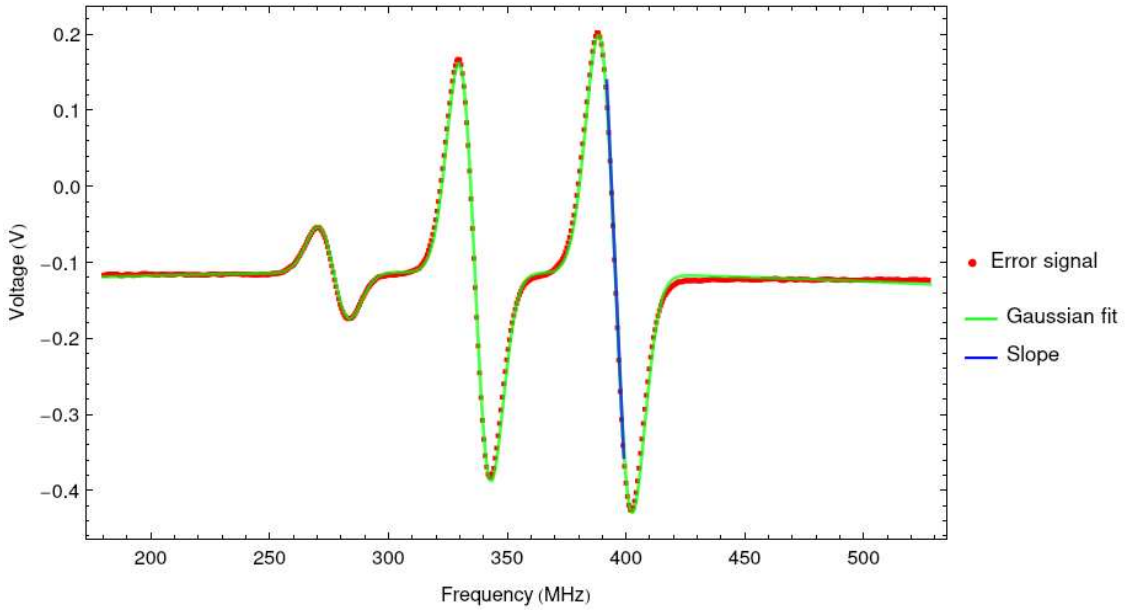

Figure 4.1: Error signal from the lock-in amplifier as the laser frequency is scanned.

Lorentzian lineshapes. Therefore, we might expect some improvements in the signal by better aligning the saturated absorption setup.

Another consideration is the potential discrepancy between the error signal seen by the PID controller, and the error signal captured by the oscilloscope to which we fit. If the time constant of the lock-in amplifier is relatively long in the time scale that it takes for the PZT to scan over the feature, this may lead to distortions in the signal that would then misrepresent it. We have confirmed that using the time constant 300μs, while scanning with frequency 15 Hz, does not produce this distortion.

4.2 RMS jitter

Once we are sure that we have a faithful representation of the error signal, we are able to characterize the RMS jitter — how much, on average, the laser's frequency fluctuates from its lockpoint. The oscilloscope is capable of telling us the RMS size of the error signal about its mean.

As long as we do not exceed the 'locking range' of Figure 2.6, which is not very wide, the error signal has in fact a linear relationship with the laser's frequency difference from its lockpoint. (Much of the effort in locking the laser, and verifying the lock, consists in making sure that we are still in this range. Outside of this range, seeing close to a zero error signal means nothing with regards to the actual frequency of the laser.) To ascertain this difference, we fit a line to the closest points from the center of the third feature, which is our lockpoint, is shown in blue in Figure 4.1. The slope of this line gives us a voltage-to-frequency conversion, usually on the order of 0.1 V/MHz. In the particular signal of Figure 4.1, this

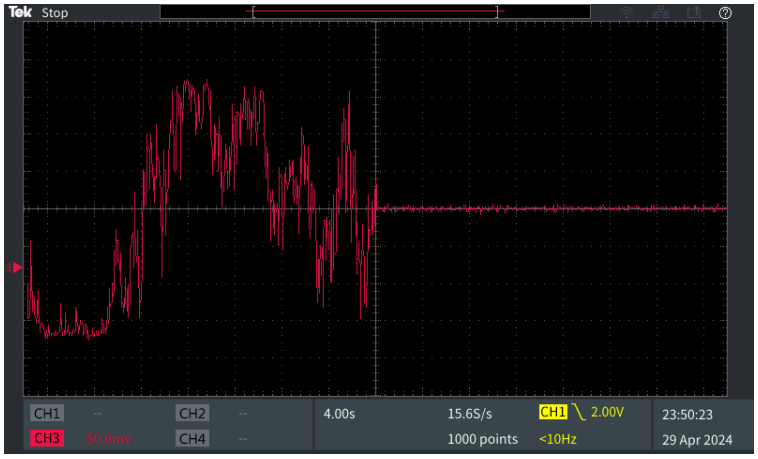

Figure 4.2: Error signal when the laser is initially unlocked, and then locked.

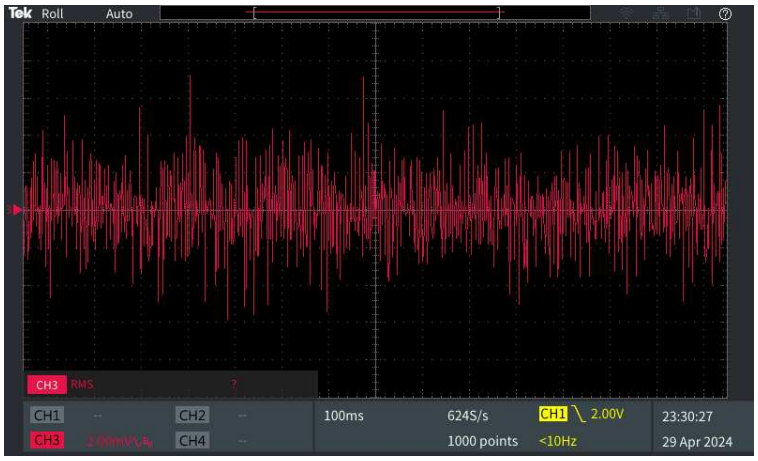

Figure 4.3: Error signal when the laser is locked. The RMS signal is ∼2mV.

was 0.069 V/MHz. Thus, when we see that the error signal has is of RMS size 2 mV, we have that the RMS jitter of laser freuqney is 2 mV / 0.069 V/MHz ≈ 29 kHz. In general, we see a ∼30 kHz jitter, unless vast alterations are made to the laser's alignment. This is more than sufficient to address the Sr^+ whose natural linewidth is $2\pi\times$ 20 MHz, and to stabilize other lasers that address other transitions of similar linewidth. We note that we believe it is possible to tune the PID coefficients more carefully, but we currently do not need to.

Chapter 5

Future work

The future is brighter than the past.

Bless Bah Awazi '24

This chapter describes the near-term goals of the lab related to the 422nm laser, which is now locked to what we expect to be near the fluorescence frequency of Sr^+.

5.1 Improving laser locks

5.1.1 PID circuitry

Currently, the laser is locked with a commerical analog PID circuit, which requires BNC cables that run across the laboratory, and thus may be picking up electromagnetic field noise along the way. We also do not require the capabilities of a commercial PID controller. Instead, we plan to add a separate, independent PID loop to our amplifier box described in Section 3.3.1 to contain our laser locking system in one place. We have a PCB for a homemade PID circuit[1], which now needs to be soldered with the correct components and tested. This circuit enables not only the tuning of P, I, and D coefficients, but also feedback polarity, internal setpoint, and output offset, and is equipped with a lock indicator.

5.1.2 Finding the accurate lockpoint

Once the 3D Paul trap is set in a working vacuum system, we can begin attempts at trapping Sr^+. To the best of our knowledge, the laser is near the $5S_{1/2} \leftrightarrow 5P_{1/2}$ transition frequency of Sr^+. The wavemeter is uncalibrated but can give us a rough estimate of laser frequency (at least up to GHz, and likely to hundreds of MHz), which is sufficient for the precision of the potentiometer of the laser controller. The locking system we have developed allow us to know that our laser can remain, after what we believe to be a 440MHz shift, at a known Rb

[1]Designed by James MacArthur, Electronics Instruments Design Lab, Harvard University.

transition frequency. The uncertainties in the center RF frequency sent to the AOM, if there are any, and the offset of the PID lock then contribute to the uncertainties in the frequency to which we are actually locked.

Without another atomic species to reference to, we cannot quantify this uncertainty nor be completely sure of the frequency of our laser, with regards to previously mentioned uncertainties. We can be sure that our laser is stable at *some* frequency. Since the linewidth of the Sr^+ transition is 20 MHz, and our laser is stable to ∼30 kHz, by scanning the frequency by modest amounts when we believe the ions have been trapped, we can verify both the exact frequency of the laser and the ability of the new 3D Paul trap to trap Sr^+ ions.

In this process, we may have to correct the offset to which we lock our PID circuit (which the MacArthur PID circuit is capable of doing), especially if we find that the 'zero' crossing of our error signal, which should be the center of the Rubidium absorption peak, is not exactly at zero. Our PID circuit currently locks to -100mV, which is a rough estimate of where our current error signal is centered. On the other hand, if we find that the shift given by AOM 1 is not exactly 440MHz, we can also correct the frequencies we send to AOMs labeled 2, 3, and 4 in Fig. 3.2. We have not yet designated dedicated RF amplifiers for those AOMs, though we know that we have enough to do so. Some of the already-built amplifiers connect with the DDS and TTL signals from our FPGA system, and at least AOMs 3 and 4 should have this capability, especially if they need a very precise detuning from each other for EIT cooling. All this requires that our laser and its components are controlled via Igor Pro.

Finally, once we have an actual ion to reference to, we can calibrate the wavemeter whose internal reference has been broken for some time.

5.1.3 Slow lock

The correction signal from the PID is currently fed to the *current* offset of the laser controller. This sets a tight bound on the maximum absolute voltage that can be sent as feedback; a correction signal that is more than a few hundred mV will cause the laser to mode hop. Currently, we have set the upper and lower limits to ±100 mV. However, as time passes, the laser is subject to perturbations and tries to drift from the lock point. If the laser stays locked, this means that the PID will at times try to counter this effect with a relatively large and constant offset. This offset can quickly exceed ±100 mV, which can lead to the laser being unlocked.

On the other hand, it is possible to make larger corrections to the *PZT* offset without encountering a mode hop. The reason that we do not use this as the primary channel for the correction signal is that it has a much slower response than the laser diode to a changing current, since the PZT changes the effective length of the laser's cavity by mechanically expanding and contracting.

We believe that we can take the advantage of the PZT offset's larger range of control by using the current offset for a fast lock, and the PZT offset for a slow lock. The latter would respond to long-term offsets in the error signal. One way to achive this slow lock

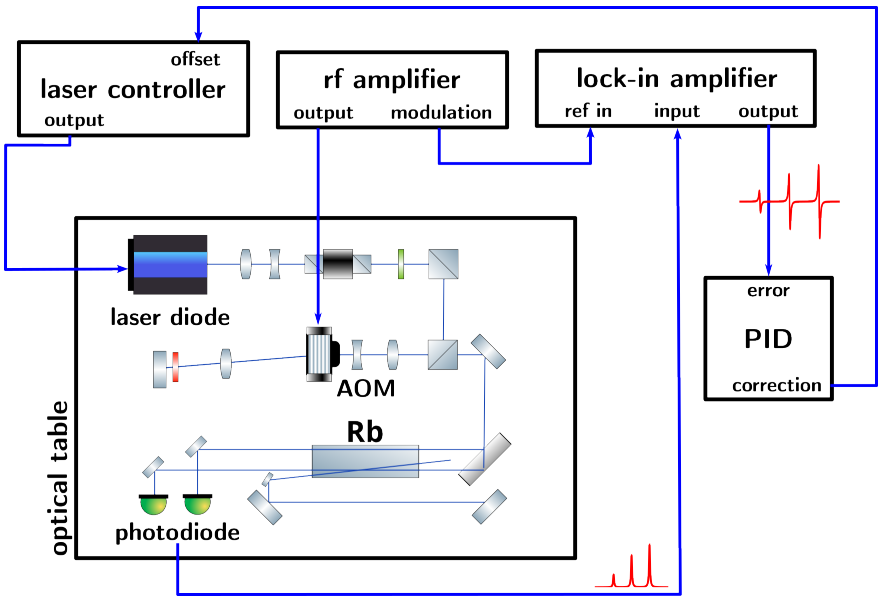

Figure 5.1: The current feedback loop that stabilizes the laser. Adding a slow lock would mean an additional control into the PZT offset of the laser controller.

would involve implementing a second feedback with a different and simpler PI circuit. We would not need the derivative circuit, since this would be a slower lock. The PI circuit would receive the correction signal from the fast lock, which still feeds into the current offset, as its error signal, and the secondary correction signal would be fed into the PZT offset. The secondary PI feedback would tend to keep the correction signal near zero so that it does not try to exceed the ± 100 mV bounds.

Alternatively, one could implement the slow 'lock' by simply nudging the PZT slightly whenever the correction signal tends to drift away from oscillating about zero. This does not even require a system as sophisticated as a PID controller; a simple software could be written where if the correction signal tends to stay at an offset, the PZT receives a slight voltage to center the correction signal closer to zero. Note that currently the 422 nm laser's lock is completely analog (except for the digital PID controller, which will one day be replaced with an analog one) and does not connect to any computer software.

5.1.4 Fabry-Perot cavity

So far, we have focused on creating and improving the lock for the 422 nm laser. We plan to use this stability in order to lock other lasers as well. Currently, the commercially stabilized HeNe laser is used to stabilize the 397 nm, 423 nm, 854 nm, 866 nm lasers, which are all used for Ca^+, in a Fabry-Perot cavity. [20] However, as the number of lasers in our lab double in order to trap another species of ions, it is no longer practical to try to stabilize both Ca^+ and Sr^+ lasers in the same cavity, referenced to the same laser.

Moreover, it is advantageous, though not strictly necessary, that we try to lock lasers

of similar wavelengths together.The locking scheme we use is *digital* — a computer receives digital data about the transmission peaks of each laser as the FP cavity length is scanned. For a laser of wavelength λ, a transmission maximum occurs every time the cavity's length increases by $\lambda/2$. The lock is achieved by trying to stabilize the 'location' of the transmission peak of the unstable laser with respect to the 'location' of the transmission peak of the stabilized laser (either the HeNe or the 422 nm), as the FP cavity is scanned. The computer then runs a PID lock to send the correction signal to the lasers.

This means that the FP cavity may have to scan longer if there was a significant difference in the wavelengths of the stabilized and unstable lasers, simply to locate the transmission peaks. Thus, we suggest that the stable HeNe and 422 nm lasers lock the following other lasers:

stabilized by:	HeNe	422 nm
Ca^+	866 nm, 854 nm	423 nm, 397 nm
Sr^+	1091 nm, 1033 nm	461 nm

The new Fabry-Perot cavity, through which the 422 nm laser could stabilize others, has not yet been completed. For more details, see Bah Awazi [10].

5.2 Sr^+ cooling and thermometry

5.2.1 EIT cooling

In order to actually implement the process to trapped Sr^+ ions, the lab must integrate both the 422nm laser (for detecting and cooling) and the 674nm laser (for thermometry) and their components into our Igor Pro system so that we can program pulse sequences. This also requires a new FPGA system, which is currently in the making.

5.2.2 Thermometry

When we refer to the 'temperature' of the ion, we divide the motional energy by the Boltzmann constant k_B for the correct dimensions. (The thermodynamic definition of temperature, as $(\partial S/\partial U)^{-1}$, strictly speaking, cannot be applied to the energy of a single ion, as definitions of microstates, macrostates, and multiplcities don't quite pertain to the state of a single isolated quanta. Of course, if we had *very many* ions, or if the single ion was coupled to an extremely complicated 'outside,' then we could define a temperature of the collection of ions.) In this sense, temperature is essentially equivalent to $\langle n \rangle$, as a measure of motional energy as the ion oscillates due to the electromagnetic fields of our trap. Note that we use the *average*, or expectation value, of the motional states that the ion is in, since we expect an isolated ion to be in a quantum superposition of different motional states.

Experimentally, how might one detect this average motional quantum number (equivalently, the average *phonon* number)? The method we can use is sometimes called resolved

sideband thermometry, since it requires resolved red and blue sidebands, or ratio thermometry, since it takes the ratio of probabilites of excitement. [21] The average phonon number, $\bar{n}$, is given in the equation,

$$\frac{P_{blue}(\uparrow;t)}{P_{red}(\uparrow;t)} = \frac{\bar{n}}{\bar{n}+1}, \tag{5.1}$$

where $P_{blue}(\uparrow;t)$ describes the probability of being excited to the upper level after a light of the blue sideband transition frequency has been applied for time t, and similarly for $P_{red}(\uparrow;t)$. This method relies on the fact that $\langle n \rangle$ is low (1 or 2) to begin with, and that we can assume the ion is in a *thermal state*, where the Boltzmann factor, $\exp\{-k_B T\}$ determines the population of state at each energy level. This would be true if the ion is at thermal equilibrium with a reservoir at temperature T.

For more details, see Dutton [9] and other literature [22] [23].

Appendix A

Seed oscillation circuitry

This appendix contains the schematic for the circuit that provides the seed oscillation for the VCO. It is a simple circuit that creates a DC offset using an inverting op-amp, an oscillation with a relaxation oscillator, another inverting op-amp to change the amplitude of the oscillation, and finally a summing amplifier to add the DC and AC components. The 'lock-in' output provides an imperfect square wave that oscillates between rougly ±15V at the same frequency as the main output oscillation. Using this circuit, create an oscillation with adjustable amplitude, frequency, and DC offsets. By altering the resistors, one can also change the range of those parameters.

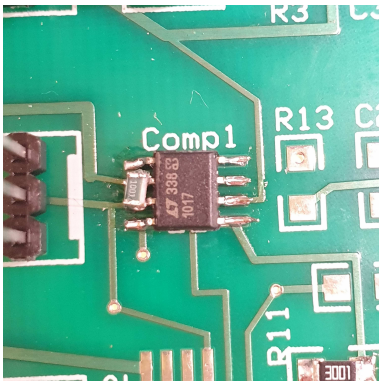

Figure A.1: The pull-up resistor, soldered on the current PCB.

We have PCBs that (almost) contain this circuit, save for one caveat. The original design was faulty because it did not include the pull-up resistor, which is required because we are using a LT1017, a comparator, for the relaxation oscillator. The pull-up resistor is included in the current circuit schematic. It is still possible to use the remaining PCBs with some very careful soldering that connects the legs 6 and 7, as seen in Figure A.1.

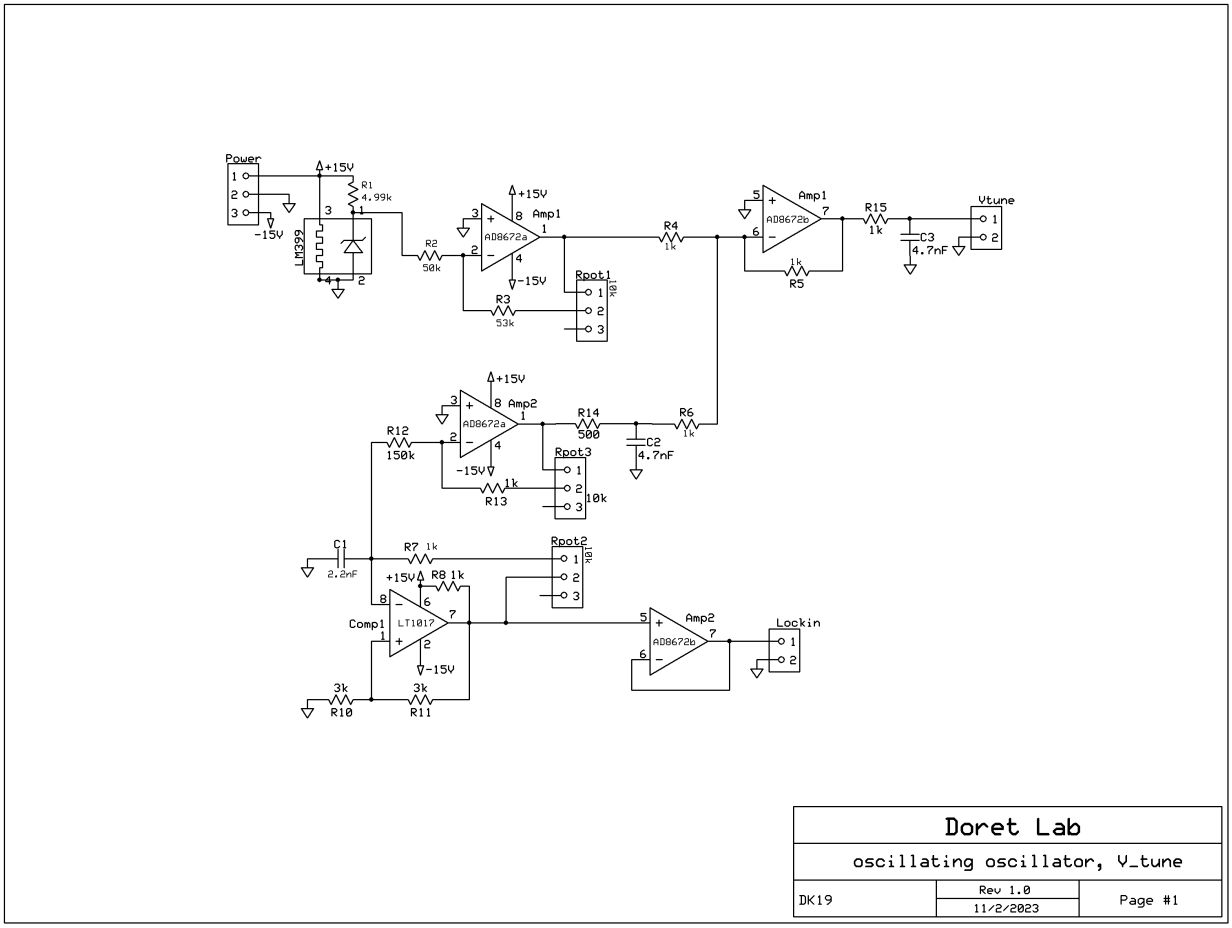
Power
+15V
R1
4.99k
LM399
-15V
R2
50k
Amp1
AD8672a
R3
53k
Rpot1
10k
R4
1k
Amp1
AD8672b
R5
1k
R15
1k
C3
4.7nF
Vtune
Amp2
AD8672a
R12
150k
R14
500
R6
1k
C2
4.7nF
Rpot3
10k
R13
1k
C1
2.2nF
R7 1k
Rpot2
10k
R8 1k
Comp1
LT1017
Amp2
AD8672b
Lockin
3k
R10
3k
R11
Doret Lab
oscillating oscillator, V_tune
DK19
Rev 1.0
11/2/2023
Page #1

Appendix B

How to lock the laser

Here are, we include some practical pointers for the process of actually locking the laser.

If the wavemeter is uncalibrated, the first thing one must do is to locate the Rb transition by monitoring the photodiodes. Usually, this will be between 710.9623–710.9630 THz on the uncalibrated wavemeter. Use a function generator to send a sawtooth wave to the PZT offset to locate the Doppler-broadened ^{85}Rb $5S_{1/2}$ (F=2) $\leftrightarrow$ $6P_{1/2}$ transition.

Once we know we are at the center of that transition, we now must try to locate the Doppler-free peaks. One way to do this is to try to see the error signals from the lock-in amplifier that looks like Figure 4.1 while still scanning the laser with a smaller amplitude. This is usually possible if one started close to the transitions, but can be difficult to find from 'far away'. In that case, it in in fact helpful to increase the RF amplifier box's ampltiude to its maximum, and see the direct signal from the photodiode (obviously, the one that sees the Doppler-narrowed peaks). Here, we are *not* scanning with the function generator at the PZT offset. So, if before, we triggered our oscilloscope to the function generator, this time we trigger the oscilloscope with the 'lock-in' output of the RF amplifier at tens of kHz. Then, by manually 'searching' the laser's frequency with the PZT dial, one will see three (two strong, one weak) jitters in the signal (it will look like the signal was surprised and 'jumped'). Those are the $F' = 2$ and $F' = 3$ transition frequencies, along with their crossover peak.

Once the correct transitions are located, we again scan the laser and see the error signal. Here is when we adjust the lock-in parameters to ensure both a strong signal without too much noise. Crucially, whatever noise there is in the error signal must not cross its center. This is also when we must note the 'zero' crossing of the signal, which is a necessary information to tuning the PID controller. Finally, before turning the PID controller on, narrow the range of the scan by decreasing the amplitude of the function generator.

The PID controller, if it succeeds in locking the laser, should be outputting a correction signal that looks like a sawtooth wave. It is trying to undo the effects of the scan. This is a sure indicator that the laser is locked, and then we are now free to turn the scan off, and the laser should remain locked. One should also be able to see on the wavemeter that the laser now prefers to stay at a much more stable frequency than before, and that there are no long-term drifts on the scale of seconds.

One should not, for example, clap, tap dance, slam the door, or kick the optical table, at least until the 'slow' lock of Chapter 5 is implemented. Perturbations that are weaker than these have occasionally unlocked the laser.

Bibliography

[1] M. A. Simón, A. Alaña, M. Pons, A. Ruiz-García, and J. G. Muga, Phys. Rev. E **103**, 012134 (2021), URL https://link.aps.org/doi/10.1103/PhysRevE.103.012134.

[2] A. Patel, Undergraduate Honors Thesis (2018).

[3] P. Robichaud, Undergraduate Honors Thesis (2021).

[4] R. Lechner, C. Maier, C. Hempel, P. Jurcevic, B. P. Lanyon, T. Monz, M. Brownnutt, R. Blatt, and C. F. Roos, Phys. Rev. A **93**, 053401 (2016), URL https://link.aps.org/doi/10.1103/PhysRevA.93.053401.

[5] R. Lechner, Ph.D. thesis, University of Innsbruck (2016).

[6] M. Ramm, T. Pruttivarasin, M. Kokish, I. Talukdar, and H. Häffner, Phys. Rev. Lett. **111**, 023004 (2013), URL https://link.aps.org/doi/10.1103/PhysRevLett.111.023004.

[7] R. Gerritsma, G. Kirchmair, F. Zähringer, J. Benhelm, R. Blatt, and C. F. Roos, The European Physical Journal D **50**, 13–19 (2008), ISSN 1434-6079, URL http://dx.doi.org/10.1140/epjd/e2008-00196-9.

[8] S. Stevenson, Undergraduate Honors Thesis (2017).

[9] S. Dutton (2024).

[10] B. Bah Awazi, Undergraduate honors thesis, Williams College, Williamstown, Massachusetts (2024).

[11] A. Kramida, Y. Ralchenko, J. Reader, and NIST ASD Team, *Nist atomic spectra database (ver 5.11) [online]*, National Institute of Standards and Technology, Gaithersburg, MD (2023), last accessed January 27, 2024.

[12] A. Shiner, Master's thesis, York University, Toronto, Ontario (2006).

[13] C. Glaser, F. Karlewski, J. Kluge, J. Grimmel, M. Kaiser, A. Günther, H. Hattermann, M. Krutzik, and J. Fortágh, Phys. Rev. A **102**, 012804 (2020), URL https://link.aps.org/doi/10.1103/PhysRevA.102.012804.

[14] C. J. Foot, *Atomic Physics* (Oxford University Press, New York, 2005).

[15] R. Das, S. Khan, T. Ravi, and K. Pandey, Eur. Phys. J. D **78** (2024).

[16] K. Sowka, M. Weel, S. Cauchi, L. Cockins, and A. Kumarakrishnan, Canadian Journal of Physics **83**, 907 (2005).

[17] J. J. Snyder, Appl. Opt. **14**, 1825 (1975), URL `https://opg.optica.org/ao/abstract.cfm?URI=ao-14-8-1825`.

[18] E. A. Donley, T. P. Heavner, F. Levi, M. O. Tataw, and S. R. Jefferts, Review of Scientific Instruments **76**, 063112 (2005), ISSN 0034-6748, `https://pubs.aip.org/aip/rsi/article-pdf/doi/10.1063/1.1930095/16000353/063112\_1\_online.pdf`, URL `https://doi.org/10.1063/1.1930095`.

[19] B. Van Der Pol, Proceedings of the Institute of Radio Engineers **18**, 1194 (1930).

[20] C. M. Meisenhelder, Undergraduate Honors Thesis (2015).

[21] A. J. Rasmusson, M. D'Onofrio, Y. Xie, J. Cui, and P. Richerme, Phys. Rev. A **104**, 043108 (2021), URL `https://link.aps.org/doi/10.1103/PhysRevA.104.043108`.

[22] D. Leibfried, R. Blatt, C. Monroe, and D. Wineland, Rev. Mod. Phys. **75**, 281 (2003), URL `https://link.aps.org/doi/10.1103/RevModPhys.75.281`.

[23] Q. A. Turchette, Kielpinski, B. E. King, D. Leibfried, D. M. Meekhof, C. J. Myatt, M. A. Rowe, C. A. Sackett, C. S. Wood, W. M. Itano, et al., Phys. Rev. A **61**, 063418 (2000), URL `https://link.aps.org/doi/10.1103/PhysRevA.61.063418`.